

# Chemical Genetics of Rapamycin-Insensitive TORC2 in *S. cerevisiae*

Joseph I. Kliegman,<sup>1,2,3</sup> Dorothea Fiedler,<sup>4</sup> Colm J. Ryan,<sup>1,2,5</sup> Yi-Fan Xu,<sup>4</sup> Xiao-yang Su,<sup>4</sup> David Thomas,<sup>4</sup> Max C. Caccese,<sup>1,2,3</sup> Ada Cheng,<sup>1,2</sup> Michael Shales,<sup>1,2</sup> Joshua D. Rabinowitz,<sup>4</sup> Nevan J. Krogan,<sup>1,2,6</sup> and Kevan M. Shokat<sup>1,2,3,\*</sup>

<sup>1</sup>Department of Cellular and Molecular Pharmacology, University of California, San Francisco, San Francisco, CA 94158, USA

<sup>2</sup>California Institute for Quantitative Biosciences, QB3, San Francisco, CA 94158, USA

<sup>3</sup>Howard Hughes Medical Institute, San Francisco, CA 94158, USA

<sup>4</sup>Department of Chemistry, Princeton University, Princeton, NJ 08540, USA

<sup>5</sup>School of Computer Science and Informatics, University College Dublin, Dublin 4, Ireland

<sup>6</sup>J. David Gladstone Institutes, San Francisco, CA 94158, USA

\*Correspondence: kevan.shokat@ucsf.edu

<http://dx.doi.org/10.1016/j.celrep.2013.11.040>

This is an open-access article distributed under the terms of the Creative Commons Attribution License, which permits unrestricted use, distribution, and reproduction in any medium, provided the original author and source are credited.

## SUMMARY

Current approaches for identifying synergistic targets use cell culture models to see if the combined effect of clinically available drugs is better than predicted by their individual efficacy. New techniques are needed to systematically and rationally identify targets and pathways that may be synergistic targets. Here, we created a tool to screen and identify molecular targets that may synergize with new inhibitors of target of rapamycin (TOR), a conserved protein that is a major integrator of cell proliferation signals in the nutrient-signaling pathway. Although clinical results from TOR complex 1 (TORC1)-specific inhibition using rapamycin analogs have been disappointing, trials using inhibitors that also target TORC2 have been promising. To understand this increased therapeutic efficacy and to discover secondary targets for combination therapy, we engineered Tor2 in *S. cerevisiae* to accept an orthogonal inhibitor. We used this tool to create a chemical epistasis miniarray profile (ChE-MAP) by measuring interactions between the chemically inhibited Tor2 kinase and a diverse library of deletion mutants. The ChE-MAP identified known TOR components and distinguished between TORC1- and TORC2-dependent functions. The results showed a TORC2-specific interaction with the pentose phosphate pathway, a previously unappreciated TORC2 function that suggests a role for the complex in balancing the high energy demand required for ribosome biogenesis.

## INTRODUCTION

Kinase signaling networks are primary regulators of cell growth and division. Improper signaling caused by mutations to kinases

is a major driver of cancer progression (Greenman et al., 2007; The Cancer Genome Atlas Research Network, 2013; Wood et al., 2007). The success of targeting single kinases has been mixed due to rapidly emerging drug resistance and significant toxicity that limits the use of several of these agents to doses that do not block cancer growth (Boss et al., 2009; Greenman et al., 2007; Haura et al., 2010; The Cancer Genome Atlas Research Network, 2013; Wood et al., 2007). In contrast, the vast majority of clinically available therapeutics have multiple targets (Knight et al., 2010; Mestres et al., 2009). Many of these off-targets contribute to the therapeutic efficacy of these drugs, but also increase their toxicity and side effects. Many preclinical and clinical studies have searched empirically for synergistic activities of kinase-targeted therapies, but systematic studies are far less common. In this study, we endeavored to systematically study synergistic interactions with target of rapamycin (TOR) kinase activity.

TOR is a primary integrator of proliferative signals, and aberrant signaling by this kinase contributes to cancer (Casadio et al., 1999; Inoki et al., 2005; Kaeberlein et al., 2005; Martin and Hall, 2005; Tee and Blenis, 2005; Tischmeyer et al., 2003). As clinical use of selective inhibitors of TOR complex 1 (TORC1; rapamycin and its derivatives, rapalogs) becomes more widespread in cancer treatment and ATP-competitive inhibitors of both TORC1 and TORC2 (including BEZ235, INK-128/MLN0128, KU-0063794, and WYE-354) reach the clinic, the search for secondary targets to use in combination therapy will gain urgency.

In addition to the clinical utility of an efficient method to find secondary targets to use in combination with TOR inhibitors, we were motivated by the fundamental lack of understanding of TORC2 biology resulting from the lack of pharmacology to selectively inhibit this complex. Although prior studies have identified roles for TORC2 in cytoskeletal reorganization, sphingolipid biosynthesis, and ribosome biogenesis (Beeler et al., 1998; Breslow et al., 2008; Helliwell et al., 1998b; Roelants et al., 2004; Schmidt et al., 1997; Zinzalla et al., 2011), it has been impossible to monitor these interactions on the rapid time-scales that are possible with drug inhibition. It has also been

impossible to specifically trace the function of these interactions to the “kinase activity” of TORC2.

Although selective pharmacological inhibition of TORC2 in mammals is not easily achieved since both TOR complexes share the same kinase, *S. cerevisiae* has two distinct kinase genes that can be independently inhibited: TOR1 and TOR2. TORC1 can contain TOR1 or TOR2 and is rapamycin sensitive. TORC2 contains only TOR2 and is rapamycin insensitive (Loewith et al., 2002). The presence of distinct TOR kinases in yeast is a key advantage that enables independent modification of the active site of Tor2 using chemical genetics to generate a selective inhibitor for a modified allele of TORC2 (Bishop et al., 2000).

To study the selective pharmacology of TORC2 inhibition, we engineered an allele of TOR2, analog-sensitive TOR2 (AS-TOR2), to accept an orthogonal kinase inhibitor that would not inhibit TORC1. To generate an unbiased map of the signaling network that TORC2 participates in, and to furnish a list of interesting secondary targets for combination therapy, we determined chemical-genetic interactions between the TORC2 kinase and ~1,000 nonessential genes in *S. cerevisiae*. For comparison, we generated a chemical-genetic interaction data set using the TORC1 inhibitor rapamycin. This approach enabled independent investigation of genetic interactions arising from the catalytic activity of either TOR complex.

Typically, genetic interactions report on how the function of one gene depends on the function of another. Negative interactions occur when two mutations cause the resulting double mutant to grow worse than expected relative to the growth rate of the two single mutants, and indicate that the two genes function in redundant or compensatory pathways. Positive interactions occur when the double mutant grows better than expected based on the phenotypes of the two single mutants, suggesting the two genes function in the same complex or in a linear pathway (Beltrao et al., 2010; Collins et al., 2007; Fiedler et al., 2009; Kelley and Ideker, 2005; Roguev et al., 2008; Ryan et al., 2012; Schuldiner et al., 2005; Tong et al., 2004). Retaining this framework for interpretation, we developed a tool for analyzing the dose-dependent effect of selective inhibitors, termed *chemical epistasis mini-array profile* (ChE-MAP).

ChE-MAP is a pharmacological extension of the powerful E-MAP technology, which typically relies on the growth phenotype of double-deletion mutants (Collins et al., 2010, 2006; Schuldiner et al., 2006) and enables dose-dependent kinase-gene interactions to be identified. The gene interactions are akin to an allelic series ranging from hypomorphic (low-dose drug treatment) to severe loss of function (high-dose drug treatment). This approach contrasts with previous E-MAPs that used drugs to either induce or modify the phenotype in double-deletion mutants (Bandyopadhyay et al., 2010). Instead, interactions in our ChE-MAP result from the combined effects of a single-deletion mutant and chemical inhibition of TOR kinase activity. This analysis enables characterization of the TOR signaling network due to rapid inactivation of either TORC1 or TORC2.

We use the ChE-MAP approach to provide an unbiased view of interactions with the catalytic function of the two TOR complexes. The results recapitulate known regulatory relationships between TORC2 and sphingolipid biosynthesis. Statistical

analysis revealed enrichment in metabolic processes, and analysis of metabolic pathways revealed an interaction network signature suggesting the involvement of TORC2 in regulating the pentose phosphate pathway (PPP). Further study showed that levels of key metabolites in the PPP decreased in response to TORC2 inhibition, but not TORC1 inhibition, suggesting a specific and previously unappreciated role for TORC2 in regulating cellular ribosides.

## RESULTS AND DISCUSSION

### A Chemical-Genetic Tool for Studying TORC2

AS kinases contain an active-site mutation, termed the gatekeeper, that allows selective inhibition with a compound that is too bulky to fit into the active site of wild-type (WT) kinases (Bishop et al., 2000). This residue is typically a branched-chain amino acid in the hydrophobic affinity pocket within the active site of the kinase (Buzko and Shokat, 2002). Mutation to a smaller residue permits binding of the bulky inhibitor.

Based on the homology of mammalian TOR (mTOR) to phosphatidylinositol 3-kinase  $\gamma$  (PI3K $\gamma$ ), we performed a structure-based alignment to identify the gatekeeper residue (I2237) of *H. sapiens* mTOR (Figure 1A). Insertion of the mTOR inhibitor BEZ235 into the active site guided by the affinity of the backbone carbonyl of V2227 to the quinoline nitrogen (the most common mode of kinase inhibitor binding) shows a steric clash with the hydrophobic pocket that is exacerbated in the presence of other branched-chain aliphatic residues, such as leucine (shown). This binding mode was confirmed in the recently published structure of mTOR bound to the structurally related inhibitor Torin2 (Yang et al., 2013). In contrast, the reported WT Tor1/2 inhibitor in yeast, QL-IX-55 (Liu et al., 2012), which contains a smaller moiety, 2-aminopyridine, in place of the quinoline moiety, shows no steric clash. We reasoned that we could mutate the gatekeeper to a smaller residue in order to make space in the hydrophobic affinity pocket to accommodate a larger inhibitor. We then performed a sequence alignment to identify the conserved leucine gatekeeper in *S. cerevisiae* Tor2 (Figure 1B). The gatekeeper residue of *S. cerevisiae* Tor2 was identified as L2178, mutated to alanine, and genetically integrated into the TOR2 locus, yielding cells containing AS-TOR2.

Since Tor2 kinase activity is essential in *S. cerevisiae*, replacement of Tor2 with a mutant that supports viability indicates that the AS-TOR2 allele is catalytically active. The nearly equivalent growth rates of WT and AS alleles in YPD (Figure S1A) indicate that the AS-TOR2 cells have a functional kinase.

Screening of the mutant kinase against a panel of ~40 ATP analogs and kinase inhibitors (Figure S1B) revealed that the AS-TOR2 allele was selectively inhibited by a single agent, BEZ235, whereas the growth of WT-TOR2 was relatively insensitive to this compound (Figure 1C). Although typical chemical scaffolds for inhibition of AS kinases based on a pyrazolo-pyrimidine scaffold (Bishop et al., 2000), or compounds designed to target the gatekeeper residue of lipid kinases (Alaimo et al., 2005) showed no activity toward AS-TOR2 (Figure S1C), BEZ235 (but not other compounds) also inhibited AS-MEC1, suggesting that this compound may be a novel and general scaffold for inhibiting AS kinases in the PIKK family.

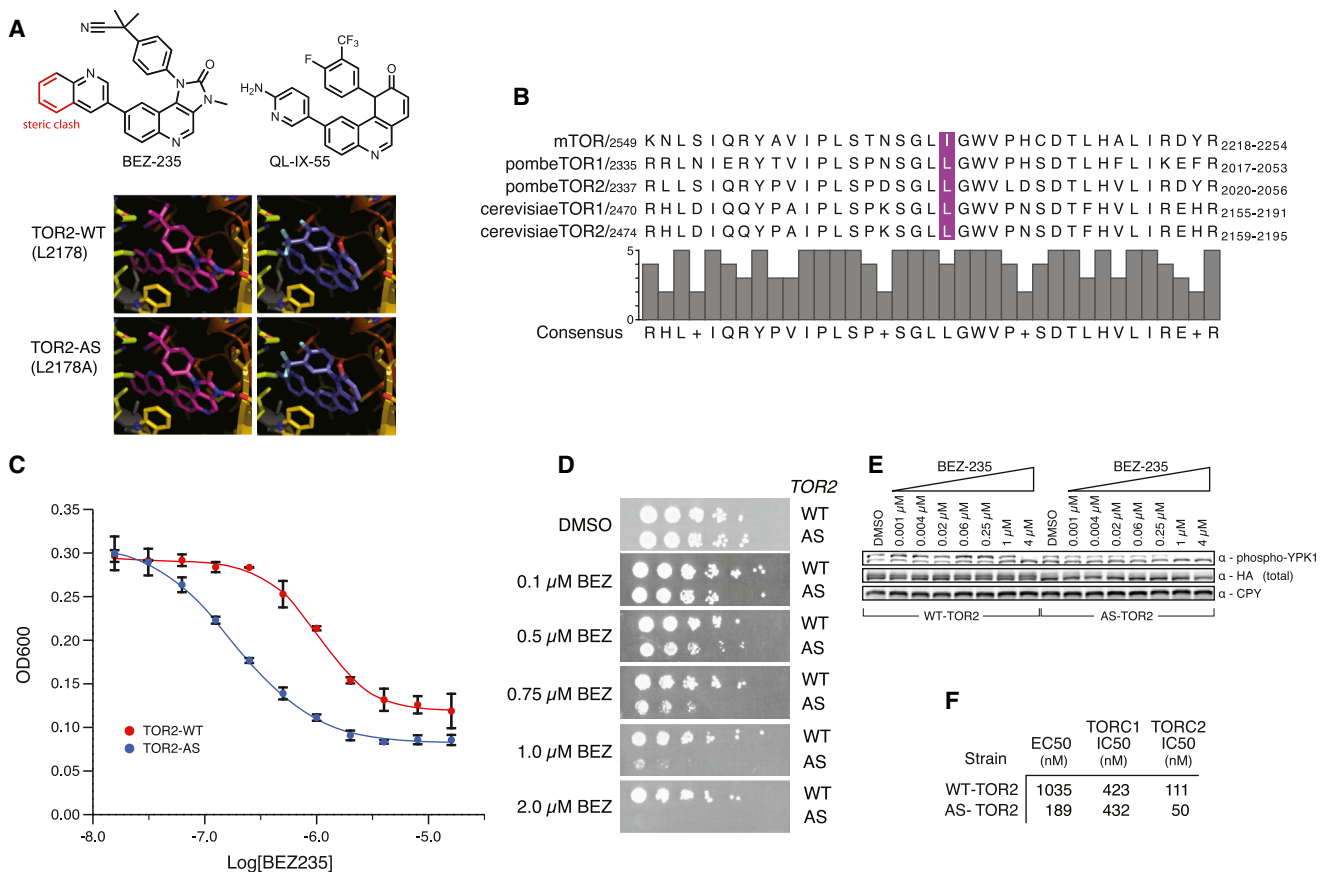


**Figure 1. Modeling and Characterization of the AS-TOR2 Allele**

(A) A homology model of mTOR based on the structure of PI3K $\gamma$  is shown with the gatekeeper residue in gray. The known *S. cerevisiae* TOR1/TOR2 inhibitors QL-IX-55 (purple) and BEZ235 (magenta) are oriented based on a typical hydrogen-bonding interaction with the backbone carbonyl of valine in the active site at van der Waals distances away from other residues that form the ATP-binding pocket. The isoleucine gatekeeper clash with BEZ235 is exacerbated by mutation to leucine and alleviated by mutation to alanine. The smaller QL-IX-55 does not sense this residue.

(B) Sequence alignment shows that the gatekeeper residue (in purple) is isoleucine in mTOR and leucine in all other cases. The active site is highly conserved.

(C) EC<sub>50</sub> of AS-TOR2 and WT-TOR2 growing in culture. AS-TOR2 is significantly more sensitive to BEZ235 than is WT-TOR2.

(D) AS-TOR2 has a growth rate identical to that of WT-TOR2 when grown on YPD. At higher doses (1 μM BEZ235), growth of AS-TOR2 is inhibited, whereas WT-TOR2 is unaffected. Growth of WT-TOR2 begins to be affected at 2 μM BEZ235.

(E) In vivo phosphorylation of Ypk1 by TORC2 in WT-TOR2- and AS-TOR2-containing cells. AS-TOR2 is significantly more sensitive to BEZ235 than is WT-TOR2.

(F) IC<sub>50</sub> values show that BEZ235 does not inhibit TORC1, AS-TOR2 does not play a significant role in the catalytic function of TORC1, and the compound selectively inhibits AS-TOR2 in TORC2 over WT-TOR2. The in vitro values correspond well to in vivo results, which are typically less sensitive due to high concentrations of ATP and the poor cell-wall permeability of yeast.

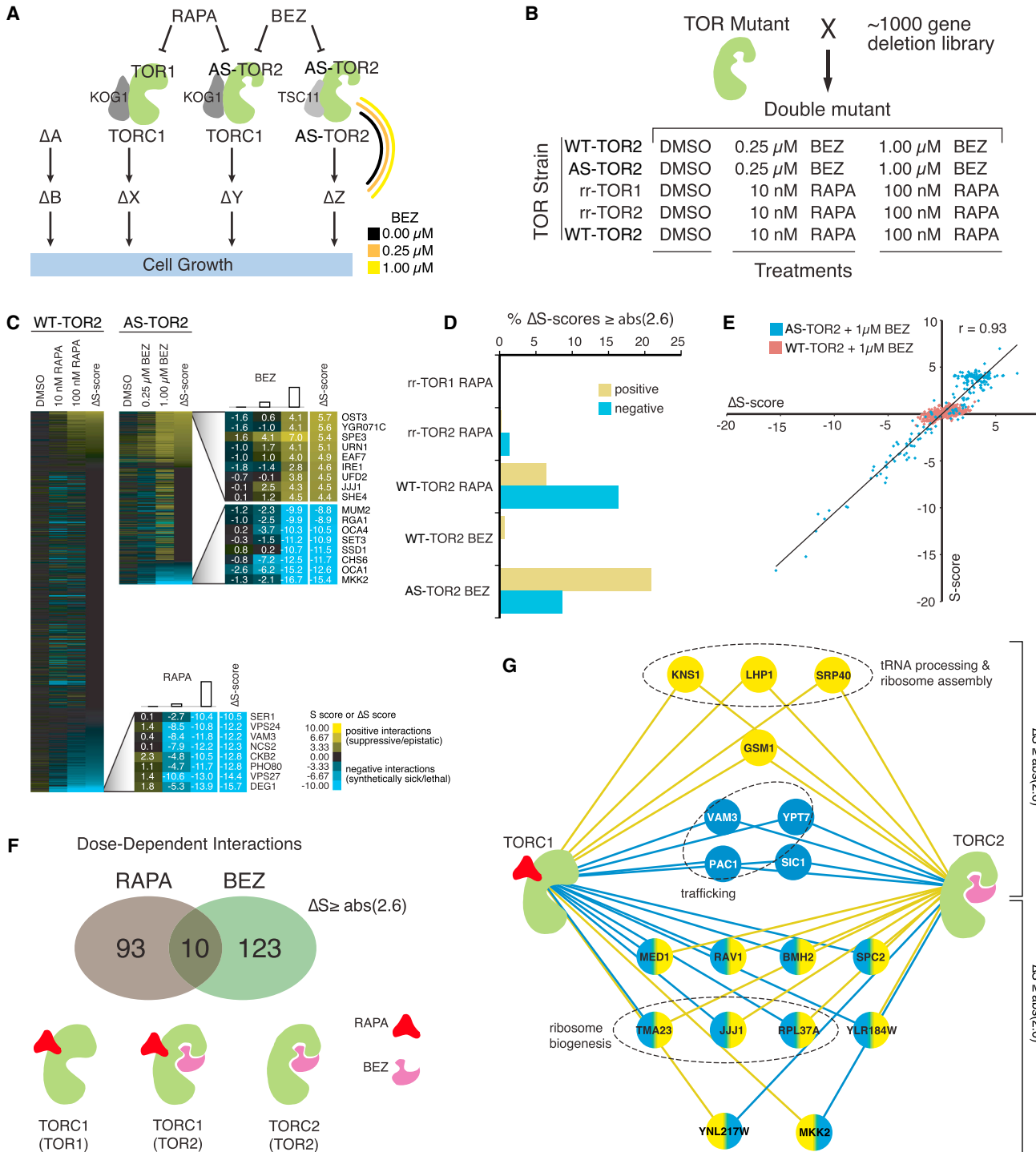
See also Figures S1, S2, and Table S5.

Although BEZ235 is a potent mTOR inhibitor in mammals (Maira et al., 2008), it only has activity toward WT yeast at high concentrations (Figures 1C and 1D), and mutation of Tor2 to the mTOR gatekeeper (isoleucine) does not confer sensitivity to the drug (Figure S2). This is likely due to slightly different positioning of the hinge loop in the mTOR kinase that pulls the quinolone moiety farther away from the hydrophobic pocket containing the gatekeeper residue.

In order to characterize the specificity of BEZ235 for AS-TOR2, we investigated potential off-target effects of the compound on kinases in the same family. We ruled out off-target effects of BEZ235 on essential kinases (Mss4 and Ptk1) since these would have resulted in growth inhibition of WT cells. To

test whether BEZ235 was targeting the PI3K ortholog Vps34, we made Vps34 conditionally essential in a ΔTOR1 background and observed no growth inhibition by BEZ235 (Figure S2). The compound also showed no activity toward WT-TOR1 or WT-TOR2 alleles when perturbed at high temperature or pharmacologically using rapamycin (Figure S2).

To test the selectivity of BEZ235 for AS-TOR2, we measured the cellular EC<sub>50</sub> of AS-TOR2 in liquid culture. The EC<sub>50</sub> of AS-TOR2 is 189 nM compared with an EC<sub>50</sub> of 1,035 nM for WT-TOR2 (Figure 1C). Since we planned to do many experiments on agar plates, we also performed a dose series from 0.1 to 2.0 μM BEZ235 (Figure 1D). The results show potent inhibition of the AS-TOR2 strain and only a slight growth defect in

**Figure 2. Chemical Epistasis Mapping of TORC1 and TORC2**

(A) TOR1 exists only as a member of TORC1. TOR2 may exist as a member of either TORC1 or TORC2. Rapamycin selectively inhibits TORC1. BEZ235 is selective for the AS-TOR2 allele. Chemical-genetic interactions behave as traditional double-deletion mutants. For interacting genes, a directional shift between the DMSO control and the (high) drug screen should occur. Dose-dependent positive interactions occur between genes in linear pathways, and dose-dependent negative interactions occur between genes in parallel pathways.

(B) TOR mutant strains were mated to a library of ~1,000 nonessential single-deletion mutants. The resulting double mutants were grown on plates containing DMSO or increasing concentrations of rapamycin or BEZ235.

(legend continued on next page)

WT-TOR2 cells at the highest concentration. In order to verify that these effects were due to selective inhibition of TORC2 in vivo, we compared the phosphorylation of the well-characterized TORC2 substrate, Ypk1, in WT-TOR2 cells and AS-TOR2 cells. Although phospho-Ypk1 does not show significant inhibition until 4  $\mu$ M BEZ235 in WT cells, it does show significant inhibition at 0.25  $\mu$ M in AS-TOR2 cells (Figure 1E).

To assess whether this sensitivity was due to the Tor2 kinase, we performed in vitro kinase assays using TORC2 purified (with hemagglutinin (HA)-tagged Tsc11, a TORC2-specific component) from cells containing AS-TOR2 or WT-TOR2. The kinase assay shows that the IC<sub>50</sub> of BEZ235 for TORC2 is 50 nM, whereas the IC<sub>50</sub> for WT is 111 nM (Figures 1F and S2). The potency was measured at 100  $\mu$ M ATP. Since the mutation commonly increases the K<sub>M</sub> for ATP (Zhang and Shokat, 2007), the decrease in competition with ATP would further enhance the efficacy of BEZ235 in cells.

Two potentially complicating factors in our analysis of TORC2 function through inhibition of AS-TOR2 were (1) the presence of Tor2 in TORC1 (Loewith et al., 2002) and (2) the possibility that BEZ235 might simply inhibit TORC1 in the presence of a slightly weaker AS-TOR2 allele. To test whether TOR2 is a major contributor to the activity of TORC1, and whether BEZ235 inhibited TORC1, we purified TORC1 from AS-TOR2 and WT-TOR2 cells. We found that the IC<sub>50</sub> of BEZ235 for TORC1 purified from WT cells is 423 nM. This IC<sub>50</sub> is too weak to account for the potent growth inhibition of AS-TOR2, since there is at least a 5-fold and sometimes a 100-fold shift in potency from in vitro IC<sub>50</sub> to in vivo EC<sub>50</sub> due to cellular competition with ATP and the poor permeability of the cell wall in yeast. This indicates that BEZ235 does not inhibit TORC1, particularly at the concentrations used in this study. Furthermore, the IC<sub>50</sub> of BEZ235 for TORC1 purified from AS-TOR2-containing cells (432 nM) indicates that there is no significant inhibition of any AS-TOR2 that may participate in TORC1 (Figures 1F and S2).

Finally, to assess whether BEZ235 inhibits TORC1 in vivo, we compared the phosphorylation of the TORC1 substrate Sch9 at T737 (Urban et al., 2007) in cells containing both WT-TOR2 and AS-TOR2. We did not observe a significant difference in Sch9 phosphorylation between the two strains, indicating that BEZ235 does not inhibit TORC1 (Figure S2), whereas rapamycin did block Sch9 phosphorylation equivalently in both WT-TOR2 and AS-TOR2 cells.

To characterize the genetic interactions resulting from selective inhibition of TORC1, we performed screens with the WT

allele in the presence of rapamycin and with the AS-TOR2 allele in the presence of BEZ235. These data sets shed light on the distinct signaling networks of TORC1 and TORC2 and provide an unbiased and selective investigation of genetic interactions with TORC2 kinase activity (Figure 2A).

### A Global Map of Genetic Interactions with the TOR2 Kinase

To systematically investigate synergistic interactions with TORC1 and TORC2, we combined our chemical-genetic tool with high-throughput yeast genetics to quantitatively assess the strength of synergistic interactions against a broad set of deleted genes. We systematically crossed either WT-TOR2 or the AS-TOR2 allele with a library of ~1,000 nonessential deletion mutants and selected for haploid double-mutant strains (Figure 2B). By growing strains on synthetic complete media containing either DMSO or increasing concentrations of rapamycin or BEZ235, we were able to measure dose-dependent growth phenotypes of mutant yeast colonies and use these phenotypes to compute individual genetic interaction scores. These screens were done in tandem with many other queries (Table S1) to ensure the robust statistics that are required for calculation of S scores (Collins et al., 2006, 2010; Schuldiner et al., 2006).

To evaluate the strength of the chemical-genetic interaction with either TOR complex, we computed S scores for all observed strains. An S score is a quantitative assessment of the strength and reproducibility of the interaction between two alleles (Collins et al., 2006, 2010). For interactions that showed a consistent and directional trend in correlating with drug dose, we calculated a difference score  $\Delta S$  ( $\Delta S = \text{High Drug} - \text{DMSO}$ ). Since  $\Delta S$  is a close analog to S score, and S = 2.6 has been used as a cutoff for significance in published literature (Fiedler et al., 2009), we chose  $\Delta S \geq |2.6|$  as a cutoff for significance in our analysis.

Three of these data sets are experimental controls for off-target effects of the compounds (Figure 2B). WT-TOR2 and AS-TOR2 cells were treated with the same concentrations of BEZ235, and rapamycin-resistant (rr) alleles (Cafferkey et al., 1993; Heitman et al., 1991; Helliwell et al., 1994) of TOR1 and TOR2 (S1972I-TOR1 and S1975I-TOR2) were treated with rapamycin. The limited number of genes that showed dose-dependent interactions with the drug-resistant alleles were filtered from the experimental data sets. The two experimental data sets reveal dose-dependent genetic interactions between specific yeast genes and rapamycin or BEZ235 (Figure 2C; Table

(C) ChE-MAP for rapamycin-treated and BEZ235-treated data sets sorted according to  $\Delta S$  score. The strengths of positive and negative chemical-genetic interactions (S scores) are reported by yellow or blue squares, respectively. Inset: top hits from each set. The AS-TOR2 data set is significantly smaller because many strains were very sick at the highest concentration of BEZ235 and were removed during quality filtering.

(D) Experimental data sets (WT-TOR2+rapa and AS-TOR2+BEZ) and control data sets (rr-TOR1+rapa, rr-TOR2+rapa, and WT-TOR2+BEZ) are shown by percent of total interactions in the data set above  $\Delta S \geq |2.6|$ . Positive interactions are in yellow, negative interactions are blue. Rapamycin and BEZ235 are selective for their intended targets and generate few off-target interactions.

(E) A scatterplot of  $\Delta S$  score versus S score illustrates the specific effect of BEZ235 on AS-TOR2. WT-TOR2 (red) is unaffected by the compound and clusters around 0. AS-TOR2 (blue) is strongly affected and shows a direct relationship between  $\Delta S$  score and S score at 1  $\mu$ M BEZ235.

(F) Number of dose-dependent genetic interactions above  $\Delta S \geq |2.6|$  in each set; 104 interactions were recorded for rapamycin and 134 were recorded for BEZ, with an overlap of ten.

(G) Network illustrating genes that hit both TORC1 and AS-TOR2 above the specified threshold. Nodes and edges are colored yellow for positive or blue for negative interactions with the indicated complex.

See also Figures S2, S3, and Tables S1, S2, S3, and S5.

S2). The examined library of yeast genes included genes from all functional categories, including regulatory proteins, signaling machinery, cell-cycle regulators, and metabolic enzymes (Table S2).

### Characteristic Dose-Dependent ChE-MAP Interactions

Analysis of ChE-MAPs generated with WT cells mated to deletion mutants and grown on 0, 0.25, or 1  $\mu$ M of BEZ235 shows that the compound is selective for the AS allele, with few off-target effects (Figure 2D). Only three dose-dependent genetic interactions are seen above  $\Delta S \geq |2.6|$  in the WT data set, suggesting that our method identifies few false positives. We analyzed the distribution of S scores for WT-TOR2 and AS-TOR2 at 1  $\mu$ M BEZ235 (Figure 2E). Based on previous E-MAP data sets, our expectation was that WT-TOR2 would show characteristic single-mutant phenotypes with S scores at or near zero. This phenotype should persist at all drug doses if BEZ235 is selective for AS-TOR2. At the highest dose of BEZ235, we observe a clear direct relationship between the S score and  $\Delta S$  in cells containing AS-TOR2. In contrast, the distribution observed when 1  $\mu$ M BEZ235 is applied to the WT-TOR2 is clustered around zero, as expected. Although the S score is a useful reference for quantification, it does not report on dose-dependent interactions, nor does it allow filtering of genetic interactions that are not due to changes in the catalytic activity of TOR. By relying on  $\Delta S$ , we are able to selectively capture dose-dependent interactions.

Few dose-dependent interactions were observed in crosses with rapamycin- or BEZ235-resistant alleles. The interactions observed were due to allelic effects from the resistance marker. The rr-TOR1 showed no dose-dependent genetic interactions upon drug treatment. With the rr-TOR2 allele, seven genes (*YPL150W*, *CKA2*, *BRE1*, *YPT7*, *IPK1*, *OPI11*, and *THP3*) showed chemical-genetic interactions above threshold. Dose-dependent interactions with the rr-TOR2 allele arose from rapamycin inhibition of WT-TOR1 in TORC1. These results are consistent with our in vitro data indicating that TOR1 is the primary kinase responsible for the outputs of TORC1.

We identified 226 dose-dependent ChE-MAP interactions with rapamycin and BEZ235 treatment at our cutoff of  $\Delta S \geq |2.6|$ . We observed 103 rapamycin-specific dose-dependent interactions and 123 TORC2-specific interactions, with an overlap of ten genes that showed a dose-dependent effect with both (Figures 2F and S3). Eight of these shared interactions showed a dose-dependent effect that was the same whether TORC1 or TORC2 was inhibited (Figure 2G). We infer that the positive interactions that arise are due to a shared function of both complexes. The four negative interactions were compensatory with both TORC2 and TORC1. Two genes (*RAV1* and *TMA23*) showed positive interactions ( $\Delta S > 2.6$ ) with TORC2 and negative interactions ( $\Delta S < -2.6$ ) with TORC1.

When we relaxed our cutoff to  $\Delta S \geq |2.0|$ , we identified eight additional dose-dependent interactions that were common to both the rapamycin and BEZ235 data sets (Figure 2G and S3). Six genes (*MED1*, *BMH2*, *RPL37A*, *JJJ1*, *SPC2*, and *YLR184W*) showed positive interactions with TORC2 and negative interactions with TORC1. Two genes (*MKK2* and *YNL217W*) were negative with TORC2 and positive with TORC1. The network

view provides a full account of dose-dependent interactions observed with each TOR complex.

Several genes that interact with both TORC1 and TORC2 play important roles in ribosomal maturation. Our results show strong positive interactions with *KNS1*, *LHP1*, and *SRP40*, all of which participate in tRNA processing and ribosome maturation (Figure 2G), suggesting an important role for both TORC1 and TORC2 in these processes. Although the role of TORC1 in phosphorylation of ribosomal protein S6 (*RPS6*) via S6-kinase (S6K) is known (Feldman et al., 2009; Richardson et al., 2004; Urban et al., 2007), the involvement of TORC2 was not appreciated until recently (Zinzalla et al., 2011). Our data support a role of TORC2 in ribosome biogenesis, since two genes (*TMA23* and *JJJ1*) involved in ribosome biogenesis (Fleischer et al., 2006; Meyer et al., 2007) and a ribosomal protein (*RPL37A*) show strong positive interactions with TORC2 while simultaneously showing strong negative interactions with TORC1 (Figure 2G). This indicates that these genes are in a pathway with TORC2 and provides additional evidence that ribosomal biogenesis plays a role in regulating TORC2 (Zinzalla et al., 2011).

### Enrichment of Sphingolipid Biosynthesis in TORC2 ChE-MAP Hits

Next, we looked in our data sets for well-characterized signaling pathways downstream of TORC2. The sphingolipid biosynthesis pathway is the best-characterized pathway under the control of TORC2 (Aronova et al., 2008; Beeler et al., 1998; Tabuchi et al., 2006). TORC2 is known to directly phosphorylate and regulate Ypk1/2 (Aronova et al., 2008; Kamada et al., 2005; Niles et al., 2012), and Ypk1/2 in turn phosphorylates and inactivates Orm1 and Orm2, which negatively regulate sphingolipid biosynthesis (Breslow et al., 2010; Niles et al., 2012; Roelants et al., 2011; Sun et al., 2012). We found extensive evidence indicating that genes involved in sphingolipid biosynthesis interact positively with the kinase activity of TORC2 (Figure 3A).

The dose-dependent chemical-genetic interactions between TORC2 and sphingolipid biosynthesis serve as a biological benchmark for the ChE-MAP technique. We observed strong dose-dependent chemical-genetic interactions between TORC2 and *ORM2* (+3.4), *DPL1* (+3.9), *LCB4* (+4.2), and *ISC1* (+4.4), all of which play integral roles in the pathway (Figure 3A). No interaction was observed with TORC1, in good agreement with prior findings (Roelants et al., 2011; Sun et al., 2012).

To confirm this phenotype, we performed tetrad analysis with these mutants and subjected crosses corresponding to the ChE-MAP results to increasing concentrations of rapamycin and BEZ in a spot dilution assay (Figure 3B). The results show that *ORM2* shows a positive phenotype upon TORC2 inhibition. The positive genetic interactions with several members of the sphingolipid biosynthesis pathway validate ChE-MAP as a viable strategy for identifying downstream signaling pathways.

### Cellular Compartment and Process Enrichment of TORC2 Interactions

Using the ChE-MAP interaction data, we asked whether there was functional enrichment for genes annotated in a particular cellular compartment or biological process. Our results were

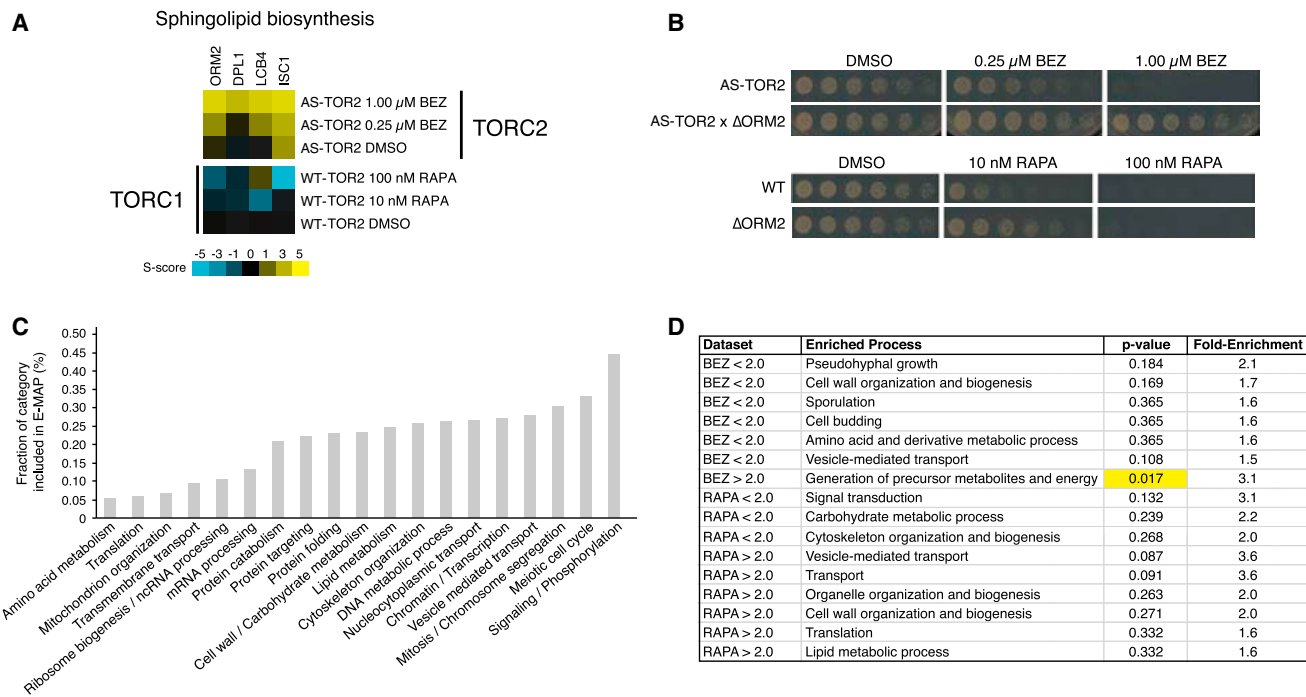


**Figure 3. Enrichment in Biological Processes**

(A) The sphingolipid biosynthesis pathway shows consistent dose-dependent behavior across all members of the pathway that were included in the screen, in good agreement with theoretical prediction. S score is indicated on a color metric scale, with blue indicating a strongly negative interaction and yellow indicating a strongly positive interaction.

(B) Genotyped and sequenced members of pulled tetrads grown on plates containing increasing concentrations of rapamycin or BEZ235 confirm phenotypes tested using the ChE-MAP.

(C) Bar graph shows the fraction of each functional biological category that was included in the E-MAP.

(D) Enrichment in either of the two data sets above or below  $\Delta S = 2.0$  was calculated using Fisher's exact test to identify terms in the cellular process GO Slim that were significantly enriched. Significant p values are highlighted in yellow.

See also Figure S3.

not biased, because we included a diverse and balanced collection of queries in the ChE-MAP (Figure 3C).

TORC2-interacting genes analyzed for enrichment in a cellular compartment using Gene Ontology (GO) (Berriz et al., 2009) terms show a 2-fold enrichment for proteins that localize to the endoplasmic reticulum (ER;  $p < 0.05$ ), controlling for sampling bias in the gene-deletion library used for this study. This result is consistent with recent work showing that mTORC2 cofractionates with the ER (Boulbés et al., 2011), and suggests that the localization of TORC2 is conserved. This expands our understanding of previous work showing that TORC2 in *S. cerevisiae* localizes to the plasma membrane and regulates sphingolipid biosynthesis (Berchtold and Walther, 2009; Berchtold et al., 2012). TORC1, by contrast, localizes in the vacuole of *S. cerevisiae* and to the lysosome surface in mammalian cells (Berchtold and Walther, 2009; Loewith et al., 2002; Zoncu et al., 2011).

Next, we analyzed the TORC1 and TORC2 data sets for enrichment of hits mapping to specific biological processes (Berriz et al., 2009). Whereas no significant enrichment was observed with TORC1 hits, significant enrichment was observed for positive hits with TORC2. The ChE-MAP showed significant enrichment ( $p < 0.05$ ) for “generation of precursor metabolites

and energy” for positively interacting TORC2 hits. Although TOR has been loosely associated with energy homeostasis due to the obvious energetic demands of protein synthesis and ribosome biogenesis, a link with metabolite synthesis was not previously shown. To investigate this further, we sought to integrate published physical interaction data with our chemical-genetic results to see whether specific metabolic processes have predominantly positive interactions with TORC2.

### Integrated Functional Network of TOR Signaling

To look for proteins involved in metabolite synthesis that physically interact with TOR, we searched for genes in metabolic GO terms that had large numbers of physical interactions with members of the TOR signaling pathway. We found that many proteins in the PPP have physical interactions with proteins in the TOR signaling pathway, which compelled us to construct a comprehensive network of PPP proteins that physically interact with each of the TOR complexes.

The network of genes that are annotated (by GO terms) to the PPP shows a distinct signature with TORC1 genes compared with TORC2 genes, as shown in Figure 4A. The figure shows that many enzymes that catalyze steps in the PPP physically interact with proteins that positively interact with AS-TOR2

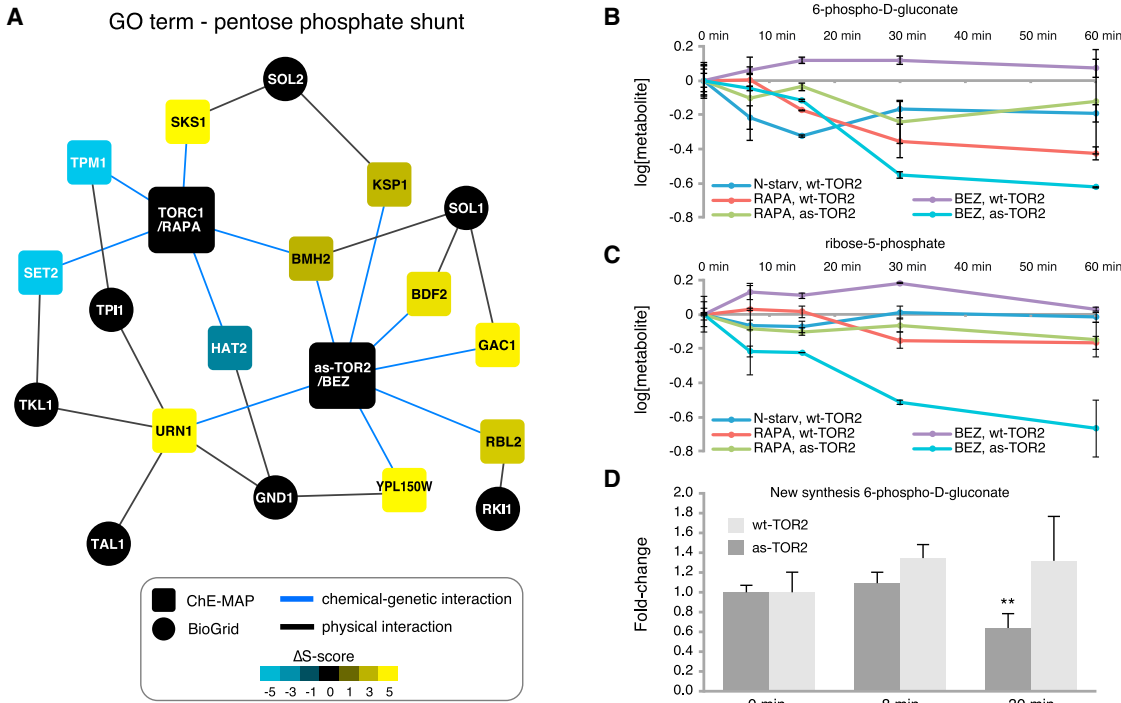


**Figure 4. Effect of Rapamycin and BEZ235 on Metabolites in the PPP**

(A) Network of ChE-MAP hits that have physical interactions with genes within the PPP GO term. Rounded rectangles and blue edges indicate chemical-genetic interactions and are colored according to the  $\Delta S$  score for the indicated gene. Enrichment for PPP-linked genes that positively interact with TORC2 is 2-fold higher than expected by random chance, with  $p = 0.02$ . Black nodes indicate genes not found in our data set (<http://thebiogrid.org>) or in previous studies (Fan et al., 2008; Fasolo et al., 2011; Graille et al., 2005; Hesselberth et al., 2006; Krogan et al., 2006; Ptacek et al., 2005; Yu et al., 2008). Black edges indicate a physical interaction.

(B) 6PG levels were quantified by LC/MS over a 60 min time course in which cells were perturbed by nitrogen starvation, inhibited with rapamycin (WT-TOR2), or inhibited with BEZ235 or rapamycin (AS-TOR2).

(C) R5P levels were quantified by LC/MS over a 60 min time course in which cells were perturbed by nitrogen starvation, inhibited with rapamycin (WT-TOR2), or inhibited with BEZ235 or rapamycin (AS-TOR2).

(D) Isotope-labeled 6PG allows direct measurement of newly synthesized metabolite in AS-TOR2 and WT-TOR2 cells, and quantification of oxPPP flux. Treatment with BEZ235 shows a significant change (\*\*) after the short 30 min time point.

In (B)–(D), error bars represent SD from the mean calculated from two independent biological replicates. See also Figure S4 and Table S4.

(*BDF2*, *GAC1*, *URN1*, and *YPL150W*). In contrast, enzymes in the PPP generally show physical interactions with proteins that negatively interact with TORC1 (*TPM1*, *SET2*, and *HAT2*). The network shows a >2-fold enrichment of positive interactions with TORC2 above what would be expected by chance alone ( $p = 0.02$ ) and predominantly negative interactions with TORC1 ( $p = \text{not significant}$ ), suggesting that the PPP is in a linear pathway with TORC2 and in either a noninteracting or parallel pathway with TORC1. This phenotype is the hallmark of a TORC2-regulated pathway, and thus we were motivated to investigate whether metabolite levels and particularly the PPP are regulated by TORC2.

#### Metabolomic Analysis of TORC1 and AS-TOR2

To test the role of TORC2 in the PPP, we used reverse-phase ion-paired liquid chromatography/mass spectrometry (LC/MS) to monitor drug-dependent changes in more than ~130 cellular metabolites, including constituents of the PPP pathway (Figure S4). Rapid metabolic changes that take place soon after drug treatment suggest direct regulation of metabolic enzymes,

whereas changes that occur on the timescale of yeast cell replication/division are more likely to indicate transcriptional changes to metabolic enzymes.

As an internal quantitative and qualitative reference for the magnitude of the metabolic changes, and a point of comparison for our drug treatment, we also assessed metabolic changes due to nitrogen starvation. Nitrogen starvation is akin to rapamycin treatment in that it disrupts the phosphorylation of TORC1 substrates (Urban et al., 2007). To identify changes in metabolite levels in response to inhibition of the TOR kinase, we treated cells with inhibitors or switched them to low-nitrogen media. We then quantified the metabolic changes over time by LC/MS to look for inhibitor-dependent changes in soluble metabolite levels.

Inhibition of TORC1 or TORC2 led to changes across all aspects of metabolism. We filtered the metabolic results to capture the change in response upon drug inhibition over the 60 min time course. After 1 hr of drug treatment, above a threshold of  $\log(\text{metabolite}) \geq |1.5|$ , nitrogen starvation showed changes in 18 metabolites out of 128 measured, rapamycin

showed changes in 24 metabolites out of 128 measured, and TORC2 treatment affected 19 out of 114 metabolites measured.

We observed that metabolic intermediates involved in the PPP were strongly downregulated in response to AS-TOR2 inhibition. In our experiments, 6-phospho-D-gluconate (6PG) and ribose-5-phosphate (R5P), two intermediates that are specific to the PPP, showed a rapid time-dependent response to treatment with BEZ235 (Figures 4B and 4C), and a slower and more modest response to rapamycin. R5P is the product of the oxidative PPP (oxPPP) and was recently shown to be produced by ribonogenesis (Clasquin et al., 2011). Although this metabolite was perturbed by the AS-TOR2 allele, the metabolite showed an additional time-dependent decrease in levels after 7 min of treatment with BEZ235. These changes may suggest a role for TORC2 in regulating both the oxidative and nonoxidative branches of the PPP.

In contrast, the delayed downregulation in response to TORC1 inhibition is consistent with previously proposed models that put enzymes in the PPP under the control of transcription factors downstream of TORC1 (Düvel et al., 2010; Robitaille et al., 2013). The rapid response upon BEZ235 treatment indicates that TORC2 may have more direct control over the PPP through kinase signaling. This hypothesis is supported by a GO analysis of the ChE-MAP (Figure 4A) that showed that seven proteins with chemical-genetic interactions with TORC2 are annotated to physically interact with metabolic enzymes of the PPP. All of these are positive interactions, indicating they are in a linear pathway with TORC2. Strong positive interactors with TORC2 include *BDF2* and *GAC1*, which both physically interact with the tRNA export protein *Sol1*, a close homolog of *Sol3/Sol4*, which catalyzes the second step of the PPP, leading to the generation of 6PG. Strong interactions are also observed between TORC2 and *RBL2*, which physically interacts with *Rki1*. *Rki1* regulates the third step in the PPP, leading to the production R5P.

To test whether TORC2 was influencing metabolite levels in the PPP by direct regulation of metabolic flux, we undertook an analysis using the tracer 1,2-<sup>13</sup>C-glucose to quantify the levels of 6PG and R5P, and to measure the relative ratio of the oxPPP and nonoxidative PPP (non-oxPPP) transketolase reaction. The rapid decrease of 6PG in the AS-TOR2 strain upon BEZ235 addition (Figure 4D) confirms TORC2's posttranslational regulation of the oxPPP, since the change in metabolite levels occurred on a rapid timescale (<30 min) as we observed previously. The lack of a substantial change of oxPPP flux in the AS-TOR2 strain relative to WT (Figure S4) upon BEZ235 treatment suggests that TORC2 does not differentially regulate oxPPP and non-oxPPP. However, it may regulate the PPP upstream of the split between oxPPP and non-oxPPP, likely through differential regulation of glucose-6-phosphate dehydrogenase (the reaction upstream of 6-phosphogluconate) and 6-phosphogluconate dehydrogenase.

## Conclusions

Yeast screens remain the most versatile tool for assessing functional genomic interactions at the organismal level. Genetic knockouts are facile for nonessential genes, but other methods are required for queries of essential genes such as the TOR kinase. Among these, decreased abundance by mRNA pertur-

bation (DAmP), temperature-sensitive (TS) degrons designed to rapidly degrade proteins at the restrictive temperature, and chemical inhibitors for a specific target are the most commonly employed techniques. The use of DAmP alleles can be unreliable due to variable levels of knockdown. TS strategies are effective but can suffer from pleiotropy. In particular, several different TS-TOR2 isolates have been reported to have widely varying effects on cell cycle, budding, and actin structures at the restrictive temperature (Helliwell et al., 1998a). Chemical inhibitors are fast acting, but the number of interesting essential targets far exceeds the number of chemical tools available to inhibit them.

In this study, we created a chemical-genetic tool that is highly specific and allows rapid inactivation of the TORC2 kinase. We used this tool to systematically and quantitatively probe the genetic interaction landscape of TORC2 kinase activity in vivo. Our method reports precisely on kinase activity and avoids the plethora of interactions that arise from destruction of protein-protein interactions.

We confirmed the robustness of our technique through positive identification of the sphingolipid biosynthesis pathway downstream of TORC2, and showed a significant enrichment in functional connections with proteins localized to the ER. Data showing enrichment for “generation of metabolites and energy” directed us to investigate the PPP with physical interaction networks that showed a pattern of interactions that is consistent with the PPP existing in a linear pathway with TORC2. By studying metabolite levels with AS-TOR2 in the presence of BEZ, we were able to observe large and rapid (<30 min) changes in metabolites that are created in the PPP, and further showed that these changes necessarily occur upstream of the transketolase reaction, since the data do not suggest a differential flux through the non-oxPPP and oxPPP.

The suggestion of a role for TORC2 in ribosomal biogenesis (Figure 2E) has interesting implications for how the cell balances energy demands to meet these needs. Emerging evidence indicates that TORC2 is an important node in ribosome biogenesis (Zinzalla et al., 2011). The high energy requirements of ribosome biogenesis create a high demand for ribose relative to NADPH, leading to activation of the PPP and production of R5P (Clasquin et al., 2011). Our evidence shows that TORC2 positively regulates metabolite synthesis in the PPP (Figure 4D) and may act as a critical relay between ribosome biogenesis and the PPP. This is particularly compelling in conjunction with evidence showing that upregulation of the non-oxPPP is required for tumor survival (Deberardinis et al., 2008).

Our approach represents a unique union of genetics and pharmacology that facilitates rapid assessment of gene-selective effects that could act as a first line of evidence in the search for synergistic therapeutics. It allows for a more granular analysis of functional genetic interactions that refer specifically to the *catalytic activity* of the kinase rather than to the scaffolding roles of the Tor protein. These findings will be a valuable resource for deciphering the different physiological functions of TORC1 and TORC2 in yeast. Such an understanding in turn may help to elucidate the roles these complexes play in mammals, where this approach cannot be directly applied, and thereby aid in the design of combination therapy regimens involving TOR inhibitors.

**EXPERIMENTAL PROCEDURES****Generation of Point Mutants**

The C-terminal region TOR1 or TOR2 (including the FAT, FRB, kinase domain, and 160 bp of the 3' UTR) was cloned onto plasmid pFA6-NAT-MX6, into the multiple cloning site immediately preceding the NAT gene (which confers resistance to nourseothricin; Werner Bioagents). AS-TOR2 (L2178A), rr-TOR2 (S1975I), and rr-TOR1 (S1972I) mutants were generated using site-directed mutagenesis. These mutants were amplified using PCR and transformed into the BY4742 strain, in which the C-terminal region of either TOR1 or TOR2 had been displaced by K.I URA3. Following selection on NAT and 5-FOA, the mutants were sequenced to confirm insertion of the desired mutations. Subsequently, the diploid mutant strains were sporulated, the Mat $\alpha$  haploid strains were selected by replica plating on selective media, and the presence of the mutation was again confirmed by sequencing.

**E-MAP Experiments**

Strain construction, plating of mutants, mutant selection, and scoring of genetic interactions (*S* scores) were performed as previously described (Collins et al., 2006; Schuldiner et al., 2005). Using a Singer Instruments pinning robot, haploid double mutants were simultaneously grown in 1,536-well format at 30°C on agar plates containing DMSO or a selective TOR inhibitor. Mutants in this study were screened in tandem with a large number of queries (Table S4) to ensure robust statistics for averaging ( $n > 30$ ). Several unrelated queries, strains containing point mutants to SCH9, WT strains containing a TOR1 marker, and a TS-TOR2 allele were used as query strains. In addition to the standard media containing G418 and NAT, plates used in the screen contained either DMSO, 0.25  $\mu$ M BEZ235, 1.00  $\mu$ M BEZ235, 10 nM rapamycin, or 100 nM rapamycin. The plates were photographed and the area of each colony was converted into pixels to quantitatively assess colony size. In untreated or treated conditions, colony sizes were based on three replicate measurements. For a given double mutant, the experimental data were used to assign a quantitative *S* score based on a modified *t* test that compares the observed double-mutant growth rate with an expected growth rate based on the average colony size across an entire plate.

**Dose-Dependent Interaction Scoring System**

Dose-dependent genetic interactions were identified for a given gene by searching for a series of *S* scores for that gene that showed a directional shift that correlated with drug concentration. The magnitude of the interaction was evaluated as the difference between the high-dose and the corresponding control strain ( $\Delta S = S \text{ score}_{\text{high drug}} - S \text{ score}_{\text{DMSO}}$ ;  $\Delta S$  scores  $\geq |2.6|$ ).

**Cellular-Compartment Enrichment of TORC2 Dose-Dependent Interactions****Enrichment of TORC2 Dose-Dependent Interactions**

Genes with a dose-dependent interaction ( $\Delta S \geq |2.0|$ ) were tested for enrichment in a specific cellular compartment. Fisher's exact test (Berziz et al., 2009) was used to identify terms in the cellular compartment GO Slim that were significantly enriched in dose-dependent hits, resulting in the observation that dose-dependent hits are  $\sim 1.6$  times more likely to be localized to the ER than expected ( $p < 0.05$  after correcting for multiple testing). The background for this calculation was all mutants with measured scores from the AS-TOR2 + BEZ235 screen, and consequently the observed enrichment is not due to the bias on the array or to data-quality filtering. The same approach was used to identify terms in the Biological Process Ontology that showed significant enrichment for dose-dependent hits. All process terms having 1.5-fold or better enrichment are shown in Figure 3.

**Tetrad Analysis**

WT-TOR2 and AS-TOR2 were mated to a single-deletion strain of interest for 48 hr prior to sporulation at room temperature for 3–5 days. The ascus was digested with zymolyase for 20 min prior to tetrad dissection. The tetrads were replica plated on selective media for genotyping, and all strains were verified using check PCR and sequencing of the TOR kinase domain locus.

**Spot Test Assay**

Overshoot cultures were grown to saturation, diluted to OD<sub>600</sub> = 0.2, and grown until all four strains had OD<sub>600</sub> = 0.8. Two-fold serial dilutions of cells were plated on DMSO; 0.1  $\mu$ M, 0.25  $\mu$ M, or 1  $\mu$ M BEZ235; or 10 nM, 50 nM, or 100 nM rapamycin. Plates were grown at 30°C and imaged after 24 hr.

**GO Network Analysis**

Circular nodes were created for all genes within a given GO term. Rectangular nodes correspond to hits in either the rapamycin or BEZ235 data sets, and circular nodes are physical binding interactions reported in the literature (Stark et al., 2006) that are absent in our screen. Genetic interactions between TORC1 or AS-TOR2 were computed and illustrated using blue edges.

**Metabolite Measurement**

The metabolome of *S. cerevisiae* was characterized as described previously (Xu et al., 2012). Saturated overnight cultures were diluted 1:30 and grown in liquid media in a shaking flask to A<sub>600</sub> of  $\sim 0.6$ . A portion of the cells (3 ml) were filtered onto a 50 mm nylon membrane filter, which was immediately transferred into  $-20^{\circ}\text{C}$  extraction solvent (40:40:20 acetonitrile/methanol/water). Serial extraction was then carried out at the indicated time points after drug treatment. Cell extracts were analyzed by reverse-phase ion-pairing LC coupled by negative-mode electrospray ionization (ESI) to a high-resolution, high-accuracy mass spectrometer (Exactive; Thermo Fisher Scientific) operated in full scan mode at 1 s scan time, 10<sup>5</sup> resolution. Compound identities were verified by exact mass and retention time matched to an authenticated standard (Melamud et al., 2010). Isomers are reported separately only when they were fully chromatographically resolved.

**Metabolic Flux Measurement**

Yeast cells were grown in 1,2-<sup>13</sup>C<sub>2</sub>-glucose in the presence of 1 nM or 5 nM estradiol. The use of 1,2-<sup>13</sup>C-glucose allows measurement of oxPPP flux. All of the isotope-labeled forms of ribose phosphate are quantitated. The flux is calculated as follows: oxPPP flux =  $(f_1 + f_2)/(f_3 + f_4 - f_0)$ , in which  $f_n$  is the labeling fraction of the  $n$ -labeled ribose phosphate. The oxidative branch of the PPP yields 1- and 3-labeled pentose phosphate. The nonoxidative branch of the PPP yields 2- and 4-labeled pentose phosphate. One molecule of 0-labeled pentose phosphate is generated for every 2- or 4-labeled pentose phosphate produced through erythrose phosphate. Therefore, 0-labeled pentose phosphate is subtracted to reflect the true flux of non-oxPPP.

**SUPPLEMENTAL INFORMATION**

Supplemental Information includes Supplemental Experimental Procedures, four figures, and five tables and can be found with this article online at <http://dx.doi.org/10.1016/j.celrep.2013.11.040>.

**ACKNOWLEDGMENTS**

The authors thank A. Roguev, H. Braberg, J. Lipp, G. Ducker, and members of the Krogan and Shokat labs for helpful comments and discussions. This work was supported by the National Science Foundation (J.I.K.), the Irish Research Council (C.J.R.), the Howard Hughes Medical Institute (K.M.S.), the NIH (GM084448, GM084279, GM081879, and GM098101 to N.J.K.), and the Sandler Family Foundation (N.J.K.). N.J.K. is a Searle Scholar and a Keck Young Investigator.

Received: January 24, 2013

Revised: July 10, 2013

Accepted: November 22, 2013

Published: December 19, 2013

**REFERENCES**

- Alaimo, P.J., Knight, Z.A., and Shokat, K.M. (2005). Targeting the gatekeeper residue in phosphoinositide 3-kinases. *Bioorg. Med. Chem.* 13, 2825–2836.

- Aronova, S., Wedaman, K., Aronov, P.A., Fontes, K., Ramos, K., Hammock, B.D., and Powers, T. (2008). Regulation of ceramide biosynthesis by TOR complex 2. *Cell Metab.* 7, 148–158.
- Bandyopadhyay, S., Mehta, M., Kuo, D., Sung, M.-K., Chuang, R., Jaehnig, E.J., Bodenmiller, B., Licon, K., Copeland, W., Shales, M., et al. (2010). Rewiring of genetic networks in response to DNA damage. *Science* 330, 1385–1389.
- Beeler, T., Bacikova, D., Gable, K., Hopkins, L., Johnson, C., Slife, H., and Dunn, T. (1998). The *Saccharomyces cerevisiae* TSC10/YBR265w gene encoding 3-ketosphinganine reductase is identified in a screen for temperature-sensitive suppressors of the Ca<sup>2+</sup>-sensitive csg2Delta mutant. *J. Biol. Chem.* 273, 30688–30694.
- Beltrao, P., Cagney, G., and Krogan, N.J. (2010). Quantitative genetic interactions reveal biological modularity. *Cell* 141, 739–745.
- Berchtold, D., and Walther, T.C. (2009). TORC2 plasma membrane localization is essential for cell viability and restricted to a distinct domain. *Mol. Biol. Cell* 20, 1565–1575.
- Berchtold, D., Piccolis, M., Chiaruttini, N., Riezman, I., Riezman, H., Roux, A., Walther, T.C., and Loewith, R. (2012). Plasma membrane stress induces relocation of SIm proteins and activation of TORC2 to promote sphingolipid synthesis. *Nat. Cell Biol.* 14, 542–547.
- Berriz, G.F., Beaver, J.E., Cenik, C., Tasan, M., and Roth, F.P. (2009). Next generation software for functional trend analysis. *Bioinformatics* 25, 3043–3044.
- Bishop, A.C., Ubersax, J.A., Petsch, D.T., Matheos, D.P., Gray, N.S., Blelhow, J., Shimizu, E., Tsien, J.Z., Schultz, P.G., Rose, M.D., et al. (2000). A chemical switch for inhibitor-sensitive alleles of any protein kinase. *Nature* 407, 395–401.
- Boss, D.S., Beijnen, J.H., and Schellens, J.H.M. (2009). Clinical experience with aurora kinase inhibitors: a review. *Oncologist* 14, 780–793.
- Boulbés, D.R., Shaiken, T., and Sarbassov, D. (2011). Endoplasmic reticulum is a main localization site of mTORC2. *Biochem. Biophys. Res. Commun.* 413, 46–52.
- Breslow, D.K., Cameron, D.M., Collins, S.R., Schuldiner, M., Stewart-Ornstein, J., Newman, H.W., Braun, S., Madhani, H.D., Krogan, N.J., and Weissman, J.S. (2008). A comprehensive strategy enabling high-resolution functional analysis of the yeast genome. *Nat. Methods* 5, 711–718.
- Breslow, D.K., Collins, S.R., Bodenmiller, B., Aebersold, R., Simons, K., Shvchenko, A., Ejsing, C.S., and Weissman, J.S. (2010). Orm family proteins mediate sphingolipid homeostasis. *Nature* 463, 1048–1053.
- Buzko, O., and Shokat, K.M. (2002). A kinase sequence database: sequence alignments and family assignment. *Bioinformatics* 18, 1274–1275.
- Cafferkey, R., Young, P.R., McLaughlin, M.M., Bergsma, D.J., Koltin, Y., Sathe, G.M., Fauchette, L., Eng, W.K., Johnson, R.K., and Livi, G.P. (1993). Dominant missense mutations in a novel yeast protein related to mammalian phosphatidylinositol 3-kinase and VPS34 abrogate rapamycin cytotoxicity. *Mol. Cell. Biol.* 13, 6012–6023.
- Casadio, A., Martin, K.C., Giustetto, M., Zhu, H., Chen, M., Bartsch, D., Bailey, C.H., and Kandel, E.R. (1999). A transient, neuron-wide form of CREB-mediated long-term facilitation can be stabilized at specific synapses by local protein synthesis. *Cell* 99, 221–237.
- Clasquin, M.F., Melamud, E., Singer, A., Gooding, J.R., Xu, X., Dong, A., Cui, H., Campagna, S.R., Savchenko, A., Yakunin, A.F., et al. (2011). Riboneogenesis in yeast. *Cell* 145, 969–980.
- Collins, S.R., Schuldiner, M., Krogan, N.J., and Weissman, J.S. (2006). A strategy for extracting and analyzing large-scale quantitative epistatic interaction data. *Genome Biol.* 7, R63.
- Collins, S.R., Miller, K.M., Maas, N.L., Roguev, A., Fillingham, J., Chu, C.S., Schuldiner, M., Gebbia, M., Recht, J., Shales, M., et al. (2007). Functional dissection of protein complexes involved in yeast chromosome biology using a genetic interaction map. *Nature* 446, 806–810.
- Collins, S.R., Roguev, A., and Krogan, N.J. (2010). Quantitative genetic interaction mapping using the E-MAP approach. *Methods Enzymol.* 470, 205–231.
- Deberardinis, R.J., Sayed, N., Ditsworth, D., and Thompson, C.B. (2008). Brick by brick: metabolism and tumor cell growth. *Curr. Opin. Genet. Dev.* 18, 54–61.
- Düvel, K., Yecies, J.L., Menon, S., Raman, P., Lipovsky, A.I., Souza, A.L., Triantafellow, E., Ma, Q., Gorski, R., Cleaver, S., et al. (2010). Activation of a metabolic gene regulatory network downstream of mTOR complex 1. *Mol. Cell* 39, 171–183.
- Fan, X., Martin-Brown, S., Florens, L., and Li, R. (2008). Intrinsic capability of budding yeast cofilin to promote turnover of tropomyosin-bound actin filaments. *PLoS ONE* 3, e3641.
- Fasolo, J., Sboner, A., Sun, M.G.F., Yu, H., Chen, R., Sharon, D., Kim, P.M., Gerstein, M., and Snyder, M. (2011). Diverse protein kinase interactions identified by protein microarrays reveal novel connections between cellular processes. *Genes Dev.* 25, 767–778.
- Feldman, M.E., Apsel, B., Uotila, A., Loewith, R., Knight, Z.A., Ruggero, D., Shokat, K.M., and Hunter, T. (2009). Active-site inhibitors of mTOR target rapamycin-resistant outputs of mTORC1 and mTORC2. *PLoS Biol.* 7, e38.
- Fiedler, D., Braberg, H., Mehta, M., Chechik, G., Cagney, G., Mukherjee, P., Silva, A.C., Shales, M., Collins, S.R., van Wageningen, S., et al. (2009). Functional organization of the *S. cerevisiae* phosphorylation network. *Cell* 136, 952–963.
- Fleischer, T.C., Weaver, C.M., McAfee, K.J., Jennings, J.L., and Link, A.J. (2006). Systematic identification and functional screens of uncharacterized proteins associated with eukaryotic ribosomal complexes. *Genes Dev.* 20, 1294–1307.
- Graillie, M., Meyer, P., Leulliot, N., Sorel, I., Janin, J., Van Tilburgh, H., and Quevillon-Cheruel, S. (2005). Crystal structure of the *S. cerevisiae* D-ribose-5-phosphate isomerase: comparison with the archaeal and bacterial enzymes. *Biochimie* 87, 763–769.
- Greenman, C., Stephens, P., Smith, R., Dalgleish, G.L., Hunter, C., Bignell, G., Davies, H., Teague, J., Butler, A., Stevens, C., et al. (2007). Patterns of somatic mutation in human cancer genomes. *Nature* 446, 153–158.
- Haura, E.B., Ricart, A.D., Larson, T.G., Stella, P.J., Bazhenova, L., Miller, V.A., Cohen, R.B., Eisenberg, P.D., Selaru, P., Wilner, K.D., and Gadgeel, S.M. (2010). A phase II study of PD-0325901, an oral MEK inhibitor, in previously treated patients with advanced non-small cell lung cancer. *Clin. Cancer Res.* 16, 2450–2457.
- Heitman, J., Movva, N.R., and Hall, M.N. (1991). Targets for cell cycle arrest by the immunosuppressant rapamycin in yeast. *Science* 253, 905–909.
- Helliwell, S.B., Wagner, P., Kunz, J., Deuter-Reinhard, M., Henriquez, R., and Hall, M.N. (1994). TOR1 and TOR2 are structurally and functionally similar but not identical phosphatidylinositol kinase homologues in yeast. *Mol. Biol. Cell* 5, 105–118.
- Helliwell, S.B., Howald, I., Barbet, N., and Hall, M.N. (1998a). TOR2 is part of two related signaling pathways coordinating cell growth in *Saccharomyces cerevisiae*. *Genetics* 148, 99–112.
- Helliwell, S.B., Schmidt, A., Ohya, Y., and Hall, M.N. (1998b). The Rho1 effector Pkc1, but not Bni1, mediates signalling from Tor2 to the actin cytoskeleton. *Curr. Biol.* 8, 1211–1214.
- Hesselberth, J.R., Miller, J.P., Golob, A., Stajich, J.E., Michaud, G.A., and Fields, S. (2006). Comparative analysis of *Saccharomyces cerevisiae* WW domains and their interacting proteins. *Genome Biol.* 7, R30.
- Inoki, K., Corradetti, M.N., and Guan, K.-L. (2005). Dysregulation of the TSC-mTOR pathway in human disease. *Nat. Genet.* 37, 19–24.
- Kaeberlein, M., Hu, D., Kerr, E.O., Tsuchiya, M., Westman, E.A., Dang, N., Fields, S., and Kennedy, B.K. (2005). Increased life span due to calorie restriction in respiratory-deficient yeast. *PLoS Genet.* 1, e69.
- Kamada, Y., Fujioka, Y., Suzuki, N.N., Inagaki, F., Wullschleger, S., Loewith, R., Hall, M.N., and Ohsumi, Y. (2005). Tor2 directly phosphorylates the AGC kinase Ypk2 to regulate actin polarization. *Mol. Cell. Biol.* 25, 7239–7248.
- Kelley, R., and Ideker, T. (2005). Systematic interpretation of genetic interactions using protein networks. *Nat. Biotechnol.* 23, 561–566.
- Knight, Z.A., Lin, H., and Shokat, K.M. (2010). Targeting the cancer kinase through polypharmacology. *Nat. Rev. Cancer* 10, 130–137.

- Krogan, N.J., Cagney, G., Yu, H., Zhong, G., Guo, X., Ignatchenko, A., Li, J., Pu, S., Datta, N., Tikuisis, A.P., et al. (2006). Global landscape of protein complexes in the yeast *Saccharomyces cerevisiae*. *Nature* 440, 637–643.
- Liu, Q., Ren, T., Fresques, T., Oppenheimer, W., Niles, B.J., Hur, W., Sabatini, D.M., Hall, M.N., Powers, T., and Gray, N.S. (2012). Selective ATP-competitive inhibitors of TOR suppress rapamycin-insensitive function of TORC2 in *Saccharomyces cerevisiae*. *ACS Chem. Biol.* 7, 982–987.
- Loewith, R., Jacinto, E., Wullschleger, S., Lorberg, A., Crespo, J.L., Bonenfant, D., Oppenheimer, W., Jenoe, P., and Hall, M.N. (2002). Two TOR complexes, only one of which is rapamycin sensitive, have distinct roles in cell growth control. *Mol. Cell* 10, 457–468.
- Maira, S.-M., Stauffer, F., Brueggen, J., Furet, P., Schnell, C., Fritsch, C., Brachmann, S., Chène, P., De Pover, A., Schoemaker, K., et al. (2008). Identification and characterization of NVP-BEZ235, a new orally available dual phosphatidylinositol 3-kinase/mammalian target of rapamycin inhibitor with potent *in vivo* antitumor activity. *Mol. Cancer Ther.* 7, 1851–1863.
- Martin, D.E., and Hall, M.N. (2005). The expanding TOR signaling network. *Curr. Opin. Cell Biol.* 17, 158–166.
- Melamud, E., Vastag, L., and Rabinowitz, J.D. (2010). Metabolomic analysis and visualization engine for LC-MS data. *Anal. Chem.* 82, 9818–9826.
- Mestres, J., Gregori-Puigjané, E., Valverde, S., and Solé, R.V. (2009). The topology of drug-target interaction networks: implicit dependence on drug properties and target families. *Mol. Biosyst.* 5, 1051–1057.
- Meyer, A.E., Hung, N.J., Yang, P., Johnson, A.W., and Craig, E.A. (2007). The specialized cytosolic J-protein, Jjj1, functions in 60S ribosomal subunit biogenesis. *Proc. Natl. Acad. Sci. USA* 104, 1558–1563.
- Niles, B.J., Mogri, H., Hill, A., Vlahakis, A., and Powers, T. (2012). Plasma membrane recruitment and activation of the AGC kinase Ypk1 is mediated by target of rapamycin complex 2 (TORC2) and its effector proteins Slm1 and Slm2. *Proc. Natl. Acad. Sci. USA* 109, 1536–1541.
- Ptacek, J., Devgan, G., Michaud, G., Zhu, H., Zhu, X., Fasolo, J., Guo, H., Jona, G., Breitkreutz, A., Sopko, R., et al. (2005). Global analysis of protein phosphorylation in yeast. *Nature* 438, 679–684.
- Richardson, C.J., Brönenstrup, M., Fingar, D.C., Jülich, K., Ballif, B.A., Gygi, S., and Blenis, J. (2004). SKAR is a specific target of S6 kinase 1 in cell growth control. *Curr. Biol.* 14, 1540–1549.
- Robitaille, A.M., Christen, S., Shimobayashi, M., Cornu, M., Fava, L.L., Moes, S., Prescianotto-Baschong, C., Sauer, U., Jenoe, P., and Hall, M.N. (2013). Quantitative phosphoproteomics reveal mTORC1 activates de novo pyrimidine synthesis. *Science* 339, 1320–1323.
- Roelants, F.M., Torrance, P.D., and Thorner, J. (2004). Differential roles of PDK1- and PDK2-phosphorylation sites in the yeast AGC kinases Ypk1, Pkc1 and Sch9. *Microbiology* 150, 3289–3304.
- Roelants, F.M., Breslow, D.K., Muir, A., Weissman, J.S., and Thorner, J. (2011). Protein kinase Ypk1 phosphorylates regulatory proteins Orm1 and Orm2 to control sphingolipid homeostasis in *Saccharomyces cerevisiae*. *Proc. Natl. Acad. Sci. USA* 108, 19222–19227.
- Roguev, A., Bandyopadhyay, S., Zofall, M., Zhang, K., Fischer, T., Collins, S.R., Qu, H., Shales, M., Park, H.-O., Hayles, J., et al. (2008). Conservation and rewiring of functional modules revealed by an epistasis map in fission yeast. *Science* 322, 405–410.
- Ryan, C.J., Roguev, A., Patrick, K., Xu, J., Jahari, H., Tong, Z., Beltrao, P., Shales, M., Qu, H., Collins, S.R., et al. (2012). Hierarchical modularity and the evolution of genetic interactomes across species. *Mol. Cell* 46, 691–704.
- Schmidt, A., Bickle, M., Beck, T., and Hall, M.N. (1997). The yeast phosphatidylinositol kinase homolog TOR2 activates RHO1 and RHO2 via the exchange factor ROM2. *Cell* 88, 531–542.
- Schuldiner, M., Collins, S.R., Thompson, N.J., Denic, V., Bhamidipati, A., Punna, T., Ihmels, J., Andrews, B., Boone, C., Greenblatt, J.F., et al. (2005). Exploration of the function and organization of the yeast early secretory pathway through an epistatic miniarray profile. *Cell* 123, 507–519.
- Schuldiner, M., Collins, S.R., Weissman, J.S., and Krogan, N.J. (2006). Quantitative genetic analysis in *Saccharomyces cerevisiae* using epistatic miniarray profiles (E-MAPS) and its application to chromatin functions. *Methods* 40, 344–352.
- Stark, C., Breitkreutz, B.-J., Reguly, T., Boucher, L., Breitkreutz, A., and Tyers, M. (2006). BioGRID: a general repository for interaction datasets. *Nucleic Acids Res.* 34 (Database issue), D535–D539.
- Sun, Y., Miao, Y., Yamane, Y., Zhang, C., Shokat, K.M., Takematsu, H., Kozutsumi, Y., and Drubin, D.G. (2012). Orm protein phosphoregulation mediates transient sphingolipid biosynthesis response to heat stress via the Pkh-Ypk and Cdc55-PP2A pathways. *Mol. Biol. Cell* 23, 2388–2398.
- Tabuchi, M., Audhya, A., Parsons, A.B., Boone, C., and Emr, S.D. (2006). The phosphatidylinositol 4,5-biphosphate and TORC2 binding proteins Slm1 and Slm2 function in sphingolipid regulation. *Mol. Cell. Biol.* 26, 5861–5875.
- Tee, A.R., and Blenis, J. (2005). mTOR, translational control and human disease. *Semin. Cell Dev. Biol.* 16, 29–37.
- The Cancer Genome Atlas Research Network (2013). Comprehensive molecular characterization of clear cell renal cell carcinoma. *Nature* 499, 43–49.
- Tischmeyer, W., Schicknick, H., Kraus, M., Seidenbecher, C.I., Staak, S., Scheich, H., and Gundelfinger, E.D. (2003). Rapamycin-sensitive signalling in long-term consolidation of auditory cortex-dependent memory. *Eur. J. Neurosci.* 18, 942–950.
- Tong, A.H.Y., Lesage, G., Bader, G.D., Ding, H., Xu, H., Xin, X., Young, J., Berzil, G.F., Brost, R.L., Chang, M., et al. (2004). Global mapping of the yeast genetic interaction network. *Science* 303, 808–813.
- Urban, J., Soulard, A., Huber, A., Lippman, S., Mukhopadhyay, D., Deloche, O., Wanke, V., Anrather, D., Ammerer, G., Riezman, H., et al. (2007). Sch9 is a major target of TORC1 in *Saccharomyces cerevisiae*. *Mol. Cell* 26, 663–674.
- Wood, L.D., Parsons, D.W., Jones, S., Lin, J., Sjöblom, T., Leary, R.J., Shen, D., Boca, S.M., Barber, T., Ptak, J., et al. (2007). The genomic landscapes of human breast and colorectal cancers. *Science* 318, 1108–1113.
- Xu, Y.-F., Zhao, X., Glass, D.S., Absalan, F., Perlman, D.H., Broach, J.R., and Rabinowitz, J.D. (2012). Regulation of yeast pyruvate kinase by ultrasensitive allostery independent of phosphorylation. *Mol. Cell* 48, 52–62.
- Yang, H., Rudge, D.G., Koos, J.D., Vaidialingam, B., Yang, H.J., and Pavletich, N.P. (2013). mTOR kinase structure, mechanism and regulation. *Nature* 497, 217–223.
- Yu, H., Braun, P., Yıldırım, M.A., Lemmens, I., Venkatesan, K., Sahalie, J., Hirozane-Kishikawa, T., Gebreab, F., Li, N., Simonis, N., et al. (2008). High-quality binary protein interaction map of the yeast interactome network. *Science* 322, 104–110.
- Zhang, C., and Shokat, K.M. (2007). Enhanced selectivity for inhibition of analog-sensitive protein kinases through scaffold optimization. *Tetrahedron* 63, 5832–5838.
- Zinzalla, V., Stracka, D., Oppenheimer, W., and Hall, M.N. (2011). Activation of mTORC2 by association with the ribosome. *Cell* 144, 757–768.
- Zoncu, R., Bar-Peled, L., Efeyan, A., Wang, S., Sancak, Y., and Sabatini, D.M. (2011). mTORC1 senses lysosomal amino acids through an inside-out mechanism that requires the vacuolar H<sup>+</sup>-ATPase. *Science* 334, 678–683.

## Supplemental Methods:

### Materials and Methods:

Drugs used in initial screening were prepared in lab following previously reported procedures or purchased from retailers. BEZ235 was purchased from LClabs ([www.lclabs.com](http://www.lclabs.com)). GFP-4EBP1 was purchased from Life Biosciences. Antibody pYpk1-T662 was generated in Ted Powers' Lab (UCD, USA). Antibody pSch9-T737 was generated in Robbie Loewith's Lab (Geneva, Switzerland).

### Strains:

The as-TOR2, wt-TOR2, rr-TOR1, and rr-TOR2 strains were derived from *S. cerevisiae* BY4742 (Mat- $\alpha$ , ura3 $\Delta$ , leu2 $\Delta$ , his3 $\Delta$ , lys2 $\Delta$ ). All strains used in ChE-MAP are marked with NAT 500bp downstream of the stop codon.

### Generation of yeast mutants:

Homologous recombination was used for generation of yeast mutants <sup>1</sup>.

### Yeast Growth assay:

One mL of overnight culture was inoculated into 50 mL of each strain (as-TOR2 and wt-TOR2) and incubated with shaking at 210 rpm at 30°C to mid-log phase. Cells were harvested by centrifugation, diluted to OD<sub>600</sub> = 0.05 and 200 $\mu$ L of the culture was seeded in 96-well plates per well. Measurements taken on a Spectra Max M5 (Molecular Devices).

### VPS34 assay:

Wild-type and  $\Delta$ TOR1 cells were grown to saturation in overnight cultures. 1mL of each culture was spread on agar plates with glass beads and dried at 30° for 30 minutes. 8 $\mu$ L of BEZ235 or DMSO was spotted on absorbent disks and incubated at either 30° or 37°. Pictures were taken after ~20 hours.

### EC50 Assay:

Wild-type and as-TOR2 cells were grown to mid-log phase, then diluted to OD<sub>600</sub> = 0.05 to start the assay. Cells were added to wells containing serial dilutions of BEZ235 so that the final concentrations ranged between 16 $\mu$ M and 4nM. Cells were grown at 30°C with constant shaking for 16 hours when readings were taken with a Spectra Max M5 (Molecular Devices). A standard non-linear dose-response curve was fit to the data using Prism 4 ([www.graphpad.com](http://www.graphpad.com)).

### In-vitro kinase assay:

TORC1 and TORC2 were purified from exponentially growing KOG1-HA (BY4742: Mata ura3 $\Delta$ , leu2 $\Delta$ , his3 $\Delta$ , lys2 $\Delta$ , KOG1-3HA, TOR2::NatMX6 )and TSC11-HA (BY4742: Mata ura3 $\Delta$ , leu2 $\Delta$ , his3 $\Delta$ , lys2 $\Delta$ , TSC11-3HA, TOR2::NatMX6 ) cells containing either wt-TOR2 or as-TOR2. Cells were grown at 30°C in YPD to mid-log phase. Cells were harvested by centrifugation, washed

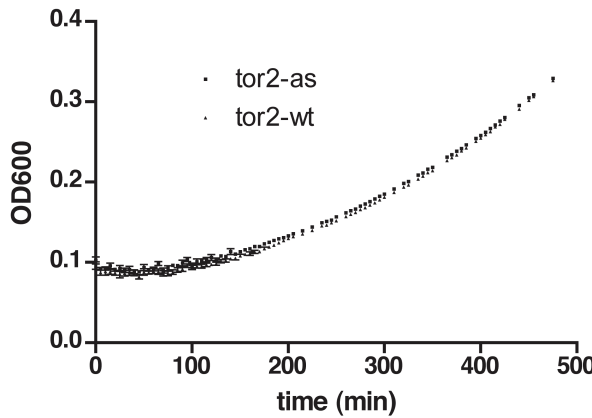
with H<sub>2</sub>O, and resuspended in lysis buffer (1x PBS pH 7, 10% glycerol, 0.5% Tween 20, protease inhibitor cocktails (Roche), phosphatases inhibitor cocktail (Sigma), and 1 mM PMSF). Equal volume of glass beads were added and cells were disrupted by bead beating at 4°C (FastPrep-120: 5x 60s at max speed). Crude lysates were cleared at 1000x g for 5 min. The extracts were precleared with Protein A Dynabeads (Life Biosciences). Protein concentrations were measured by Bradford and equal amounts of proteins were incubated with Protein A Dynabeads conjugated to monoclonal HA antibody (12CA5, Roche) overnight at 4°C. Beads were washed 4x with lysis buffer. Kinase reactions were performed in kinase buffer (1x PBS, 20% glycerol, 0.5% Tween 20, 4mM MnCl<sub>2</sub>, 10 mM DTT, protease inhibitor cocktails (-EDTA) (Roche), and phosphatases inhibitor cocktail (Sigma). BEZ235 was tested using 4-fold serial dilutions from 4μM to 0.1nM. Kinase reactions were performed in kinase buffer in a final volume of 30 μL containing 2 μg of PHAS-I (4EBP1). Kinase reactions were started with the addition of 100 μM ATP and 5 μCi [ $\gamma$ -<sup>32</sup>P]ATP, shaken for 4 hours at room temp, and terminated by cooling on ice. 20μL of the reaction was run on a 4-20% acrylamide gel. The gel was dried for 1hr at 80°C and exposed to a phosphorimaging screen overnight and imaged on a Typhoon fluorimeter. Lanes were quantified using Image J (<http://rsb.info.nih.gov/ij/>) and IC<sub>50</sub> values were determined by fitting the data to a standard non-linear sigmoid dose-response curve using the Prism 4 software package ([www.graphpad.com](http://www.graphpad.com)).

#### In-vivo Phosphorylation assays:

Cultures of HA-tagged Ypk1 or Sch9 in either wt-TOR2 or as-TOR2 background were grown to OD<sub>600</sub> = 0.9 before the culture was split and treated with 4-fold serial dilutions with a final concentration from 4μM to 0.02μM BEZ235 or 1μM to 2nM rapamycin for 20minutes at 30°C. Cells were washed 1x with H<sub>2</sub>O, treated with 100μM NaOH for 5 minutes, and lysed by vortexing in loading buffer. Samples were run on 4-20% acrylamide gel, and transferred to nitrocellulose. Membranes were probed with primary antibodies  $\alpha$ -CPY (1:10,000; Life Biosciences),  $\alpha$ -HA (1:10,000; 12CA5, Roche),  $\alpha$ -phospho-Ypk1 antibodies (1:20,000; Powers Lab, UCD), or  $\alpha$ -phospho-Sch9 antibody (1:500; Loewith Lab, University of Geneva). The  $\alpha$ -phospho-YPK1 antibody recognizes the hydrophobic motif position T662 in Ypk1. The  $\alpha$ -phospho-Sch9 antibody recognizes T737, one of five phosphorylation sites at the C-terminus of Sch9. Membranes were then probed with appropriate secondary antibodies conjugated to IRDye (1:10,000; LI-COR Biosciences) and visualized using an Odyssey Infrared Imaging System (LI-COR Biosciences).

1. Ma, H., Kunes, S., Schatz, P. J. & Botstein, D. Plasmid construction by homologous recombination in yeast. *Gene* **58**, 201–216 (1987).

A.



B.

Compound	wt-TOR2 halo	as-TOR2 halo	wt-MEC1 halo	as-MEC1 halo
DMSO	-	-	-	-
PI-121	-	-	n/a	n/a
INK1232	-	-	n/a	n/a
INK128	-	-	n/a	n/a
PI-103	-	-	n/a	n/a
LY29223	-	-	n/a	n/a
LY29223-ETHYL	-	-	n/a	n/a
LY29223-METHYL	-	-	n/a	n/a
LY29223-PROPYL	-	-	n/a	n/a
LY29223-iPr	-	-	n/a	n/a
LY29223-phenyl	-	-	n/a	n/a
LY29223-BUTYL	-	-	n/a	n/a
LY29223-BENZYL	-	-	n/a	n/a
BEZ235	-	+	-	+
3MB-PP1	-	-	-	-
3IB-PP1	-	-	-	-
3BR-PP1	-	-	-	-
STAR12	-	-	-	-
STAR26	-	-	-	-
AQ201	-	-	-	-
AQ206	-	-	-	-
FUR164	-	-	-	-
FUR174	-	-	-	-
DR042	-	-	-	-
CZ02	-	-	-	-
1NM-PP1	-	-	n/a	n/a
2NM-PP1	-	-	n/a	n/a
CZ22	-	-	n/a	n/a
BA30	-	-	n/a	n/a
BA50	-	-	n/a	n/a
BA121	-	-	n/a	n/a
BA146	-	-	n/a	n/a
PP242	-	-	n/a	n/a
ZK325	-	-	n/a	n/a
ZK327	-	-	n/a	n/a
RAPA	+	+	+	+

C.

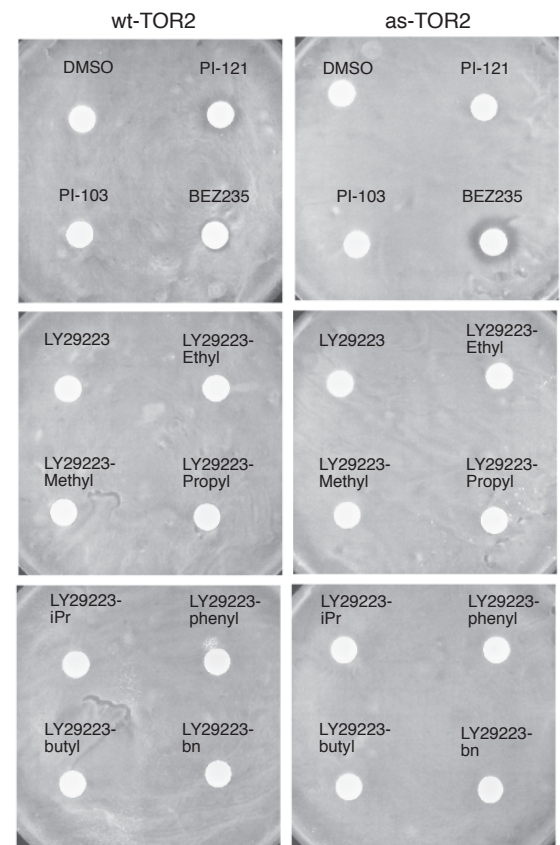


Figure S1, Related to Figure 1. Characterization of as-TOR2 growth and chemical screens.

(A) Growth of wt-TOR2 and as-TOR2 in YPD liquid cultures shown with standard deviations based on 3 measurements.  
 (B) Compounds screened against the wt-TOR2, as-TOR2, wt-MEC1, and as-MEC1 for selectivity against the analog-sensitive allele. (+) indicates sensitivity, (-) indicates insensitivity, (n/a) indicates the compound was not screened.  
 (C) The images show an example of screened plates.

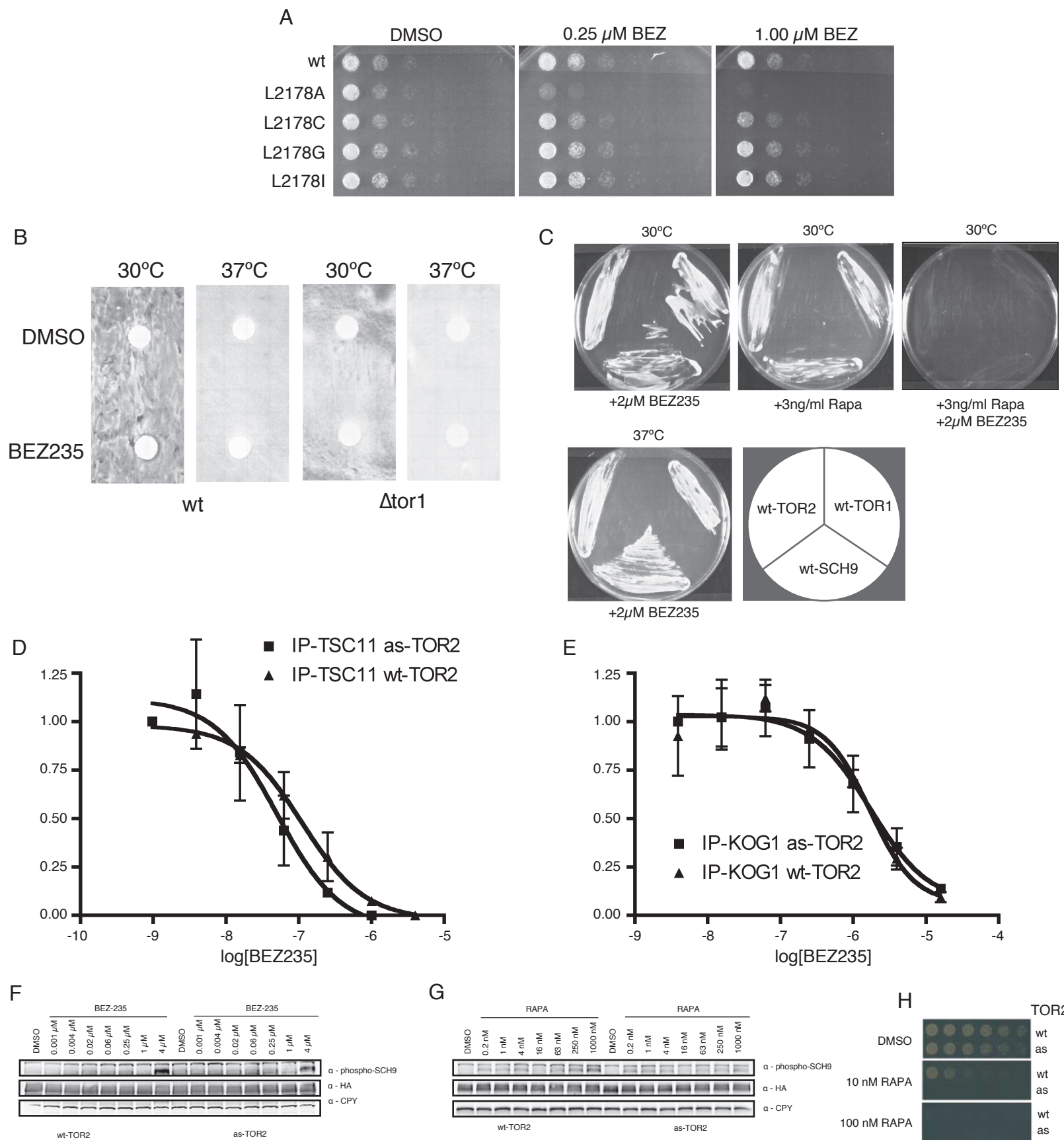


Figure S2, Related to Figures 1 & 2. Characterization of the as-TOR2 mutant. (A) Growth of several TOR2 gatekeeper mutants on YPD with increasing concentrations of BEZ235. (B) Halo assay of BEZ235 in which VPS34 is perturbed at 37°C with  $\Delta$ tor1 background. Lack of killing by BEZ235 indicates the compound does not hit VPS34 or TOR1. (C) Streak assay of wt-TOR1, wt-TOR2, wt-SCH9 with BEZ235 at 30°C and 37°C shows BEZ235 does not hit TOR1 or VPS34. Streak assay of wt-TOR1, wt-TOR2, and wt-SCH9 at 30°C with rapamycin and BEZ235 shows that marked alleles do not behave as DAmP strains (perturbed alleles). (D) IP-kinase assay shows in vitro IC50 of TORC2 is 50nM purified from as-TOR2 cells and to 111nM purified from wt-TOR2 cells. (E) IP-kinase assay shows in vitro IC50 of TORC1 is 432nM purified from as-TOR2 cells and 423nM purified from wt-TOR2 cells. (F) In vivo phosphorylation of Sch9 shows BEZ235 does not inhibit TORC1 at experimentally relevant concentrations. (G) In vivo phosphorylation of Sch9 shows TORC1 is not more sensitive to inhibition in as-TOR2 cells. (H) Spot test assay shows as-TOR2 is a perturbed allele since it is killed at a lower concentration of rapamycin than wt-TOR2.

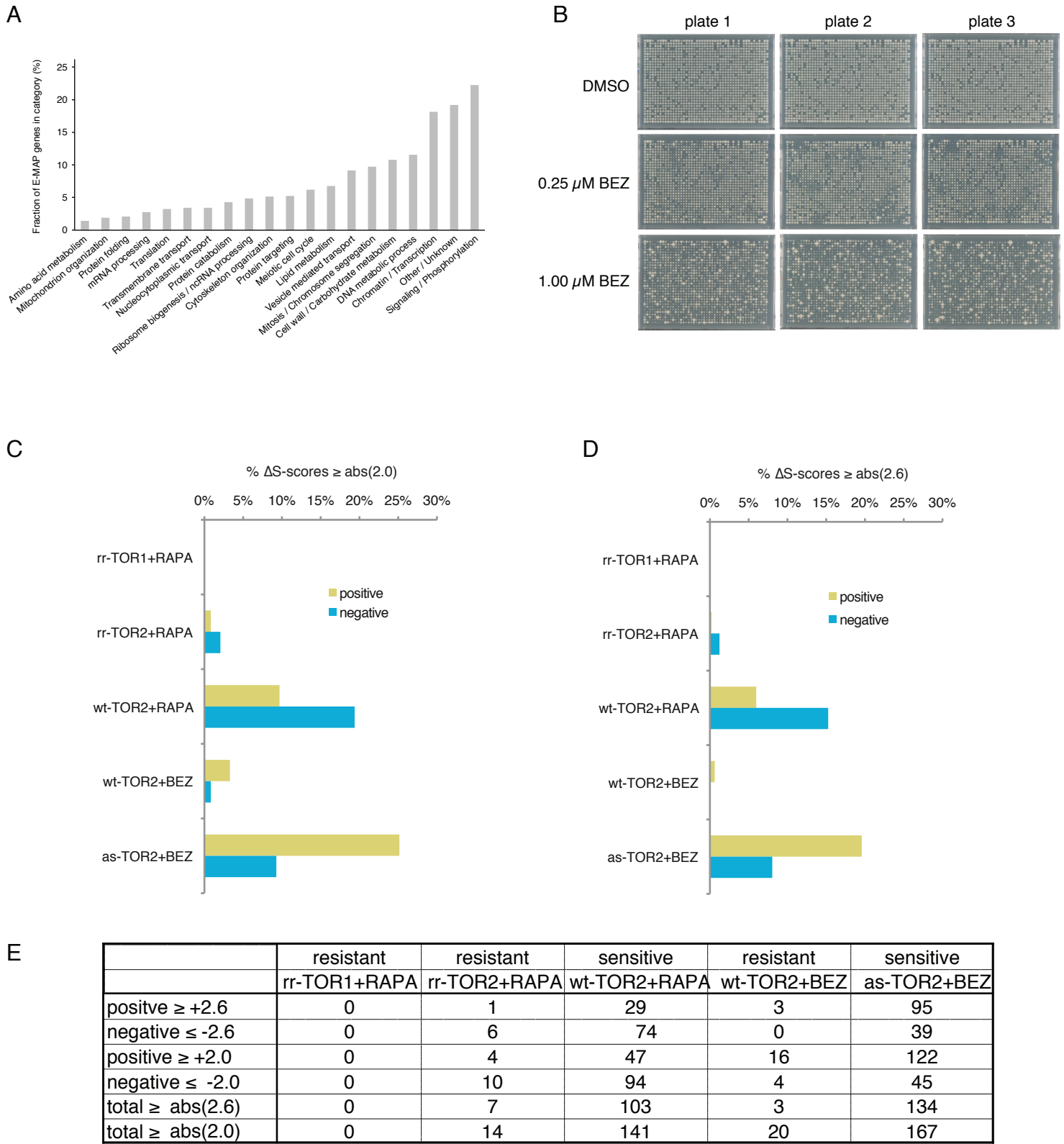
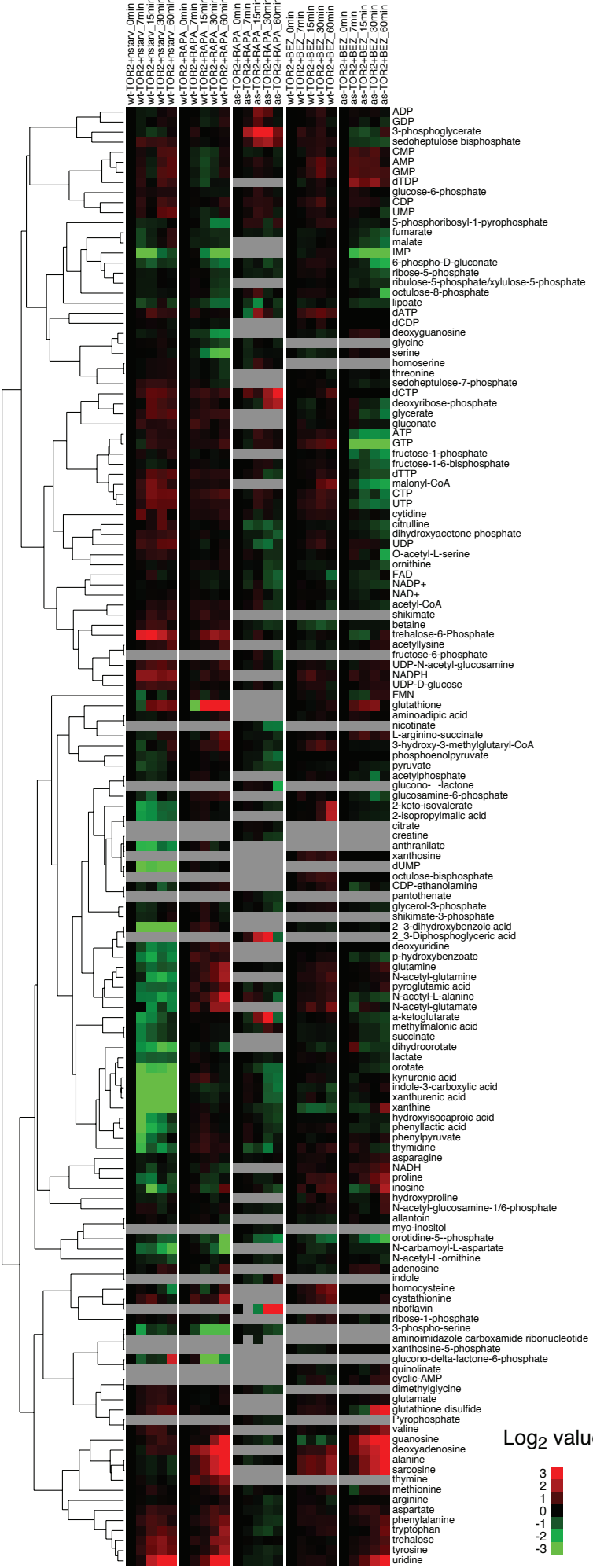


Figure S3, Related to Figures 2 & 3, ChEMAP parameters, plate pictures, and quantification.

- (A) Fraction of ChE-MAP genes in each category by percent of total genes on array
- (B) Representative plate pictures of double mutant colonies at different doses of BEZ235 after 24 hours growth at 30°C
- (C) Positive and negative hits for resistant and sensitive datasets using a threshold of  $\Delta S\text{-score} \geq \text{abs}(2.0)$
- (D) Positive and negative hits for resistant and sensitive datasets using a threshold of  $\Delta S\text{-score} \geq \text{abs}(2.6)$
- (E) Number of positive and negative hits at specified threshold for resistant and sensitive datasets



Oxidative PPP Flux

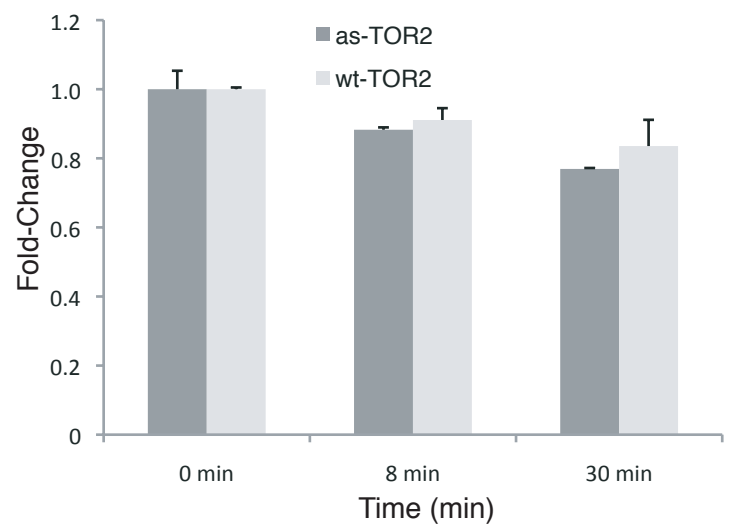


Figure S4, Related to Figure 4. Metabolomics analysis of as-TOR2 inhibition.  
(A) Heatmap showing downregulation (green) and upregulation (red) of metabolites in wt-TOR2+nitrogen starvation, wt-TOR2+RAPA, as-TOR2+RAPA, wt-TOR2+BEZ235, and as-TOR2+BEZ235 samples over a 60 minute timecourse. Metabolite levels normalized to 0 minute time point for each experiment.  
(B) Flux through oxidative PPP does not show a significant change in as-TOR2 cells relative to wt-TOR2 cells when treated with BEZ235 at short timepoints.

**Table S1, Related to Figure 2. List of Queries Used in this Study**

TOR2- L2178A +DMSO  
TOR2- L2178A +0.25 $\mu$ M BEZ  
TOR2- L2178A +1.00 $\mu$ M BEZ  
TOR2- WT + DMSO  
TOR2- WT + 0.25 $\mu$ M BEZ  
TOR2- WT + 1.00 $\mu$ M BEZ  
TOR2- WT + DMSO  
TOR2- WT + 10nM RAPA  
TOR2- WT + 100nM RAPA  
TOR1- S1972I + DMSO  
TOR1- S1972I + 10nM RAPA  
TOR1- S1972I + 100nM RAPA  
TOR2- S1975I + DMSO  
TOR2- S1975I + 10nM RAPA  
TOR2- S1975I + 100nM RAPA

**Additional Queries Used for Averaging Purposes\***

TOR1- WT + DMSO  
TOR1- WT + 0.25 $\mu$ M BEZ  
TOR1- WT + 1.00 $\mu$ M BEZ  
 $\Delta$ TOR1  
SCH9- WT + DMSO  
SCH9- WT + 2 $\mu$ M NM-PP1  
SCH9- WT + 10 $\mu$ M NM-PP1  
SCH9- WT + 50 $\mu$ M NM-PP1  
SCH9- WT + 2 $\mu$ M NM-PP1  
 $\Delta$ SCH9  
TOR1- L2174A  
TOR1- I1954V + DMSO  
TOR1- I1954V + 10nM RAPA  
TOR1- I1954V + 100nM RAPA  
TOR1- L2174A\_I1954V + DMSO  
TOR1- L2174A\_I1954V + 0.25 $\mu$ M BEZ  
TOR1- L2174A\_I1954V + 1.00 $\mu$ M BEZ

\*with the exception of  $\Delta$ TOR1 and  $\Delta$ SCH9 which gave profiles typical of these mutants, additional queries gave profiles similar to 'wild-type' or 'resistant' alleles in our study

Table S2 Related to Figure 2. S-scores and  $\Delta S$  scores for all genes that have quantified S-scores for all conditions (including all negative results).

Table S3, Related to Figure 2. S-scores and  $\Delta S$  scores for all genes that showed a directional relationship when treated with rapamycin or BEZ.

Table S4, Related to Figure 4. Relative Metabolite Levels for time course treatment upon nitrogen starvation, rapamycin treatment or BEZ235 treatment. Metabolites are normalized against drug-treated wild-type levels for as-TOR2.

Table S5, Related to Figures 1 & 1. Strains used in this study

<b>Strain</b>	<b>Used in</b>	<b>Genotype</b>	
BY4742	Fig 1-4, S1, S2, S3, S4, S5, S6, S7	Mata, ura3Δ0, leu2Δ0, his3Δ1, lys2Δ0, NatMX::TOR2	query strain
BY4741	Fig 2, 3	Mata, ura3Δ0, leu2Δ0, his3Δ1, met15Δ0, KanMX::(ARRAYΔ)	array strains
BY4742	Fig S3B	Mata, ura3Δ0, leu2Δ0, his3Δ1, lys2Δ0, NatMX::ΔTOR1	
BY4742	Fig S3D	Mata, ura3Δ0, leu2Δ0, his3Δ1, lys2Δ0, NatMX::TOR2, 6HA-TSC11::hph	
BY4742	Fig S3E	Mata, ura3Δ0, leu2Δ0, his3Δ1, lys2Δ0, NatMX::TOR2, 6HA-KOG1::hph	
BY4742	Fig 1	Mata, ura3Δ0, leu2Δ0, his3Δ1, lys2Δ0, NatMX::TOR2, 6HA-YPK1::hph	
BY4742	Fig S3F, S3G	Mata, ura3Δ0, leu2Δ0, his3Δ1, lys2Δ0, NatMX::TOR2, 6HA-SCH9::hph	